JGP Journal of General Physiology

ARTICLE

Phosphatidylinositol 4,5-bisphosphate is regenerated by speeding of the PI 4-kinase pathway during long PLC activation

Jongyun Myeong[1], Lizbeth de la Cruz[1], Seung-Ryoung Jung[2], Jun-Hee Yeon[3], Byung-Chang Suh[3], Duk-Su Koh[1], and Bertil Hille[1a]

The dynamic metabolism of membrane phosphoinositide lipids involves several cellular compartments including the ER, Golgi, and plasma membrane. There are cycles of phosphorylation and dephosphorylation and of synthesis, transfer, and breakdown. The simplified phosphoinositide cycle comprises synthesis of phosphatidylinositol in the ER, transport, and phosphorylation in the Golgi and plasma membranes to generate phosphatidylinositol 4,5-bisphosphate, followed by receptor-stimulated hydrolysis in the plasma membrane and return of the components to the ER for reassembly. Using probes for specific lipid species, we have followed and analyzed the kinetics of several of these events during stimulation of M_1 muscarinic receptors coupled to the G-protein G_q. We show that during long continued agonist action, polyphosphorylated inositol lipids are initially depleted but then regenerate while agonist is still present. Experiments and kinetic modeling reveal that the regeneration results from gradual but massive up-regulation of PI 4-kinase pathways rather than from desensitization of receptors. Golgi pools of phosphatidylinositol 4-phosphate and the lipid kinase PI4KIIIα (*PI4KA*) contribute to this homeostatic regeneration. This powerful acceleration, which may be at the level of enzyme activity or of precursor and product delivery, reveals strong regulatory controls in the phosphoinositide cycle.

Introduction

This paper concerns the dynamics of phosphoinositide membrane lipids in living cells. Polyphosphoinositides, a family of low-abundance membrane phospholipids, regulate many vital functions of the cell (Anderson et al., 2013; Balla, 2013; Traynor-Kaplan et al., 2017; Dickson and Hille, 2019). The parent compound phosphatidylinositol (PtdIns) can be phosphorylated on the 3-, 4-, and 5-hydroxyl positions of its myo-inositol headgroup to form a total of seven polyphosphoinositide species. Each has specific signaling roles. Here, we focus on dynamic changes in pools of two species, phosphatidylinositol 4-phosphate (PtdIns4*P*) and phosphatidylinositol 4,5-bisphosphate (PtdIns(4,5)P_2). These lipid species are generated from PtdIns by the sequential action of lipid kinases in the phosphatidylinositol 4-kinase (PI4K) and phosphatidylinositol 4-phosphate 5-kinase (PIP5K) families (Fig. 1). The phosphorylation can be removed by lipid 4- and 5-phosphatases. PtdIns(4,5)P_2 is also hydrolyzed and depleted by activation of phospholipase Cβ (PLCβ) at the plasma membrane (PM) during stimulation of G_q-coupled receptors. This cleavage generates two potent second messengers, inositol trisphosphate (Ins(1,4,5)P_3), which enters the cytoplasm, and diacylglycerol (DAG), which remains in the membrane. PtdIns4*P* is likely also a substrate of PLCβ.

Individual phosphoinositides occupy the cytoplasmic leaflet of specific subcellular membranes (Fig. 1): PtdIns, the most abundant phosphoinositide, is on most intracellular membranes but quite sparse on the PM (Pemberton et al., 2020; Zewe et al., 2020); PtdIns4*P* is on the PM, Golgi, and secretory, transport, and endo/lysosomal vesicles; and PtdIns(4,5)P_2 is predominantly on the PM and serves as a signature lipid for that membrane (Balla, 2013; Hammond et al., 2014). Beyond being the precursor of Ins(1,4,5)P_3 and DAG second messengers, PM PtdIns(4,5)P_2 is a required regulatory cofactor for numerous pumps and transporters as well as for exocytosis and endocytosis (Hille et al., 2015). In addition, receptor-mediated depletion of PtdIns(4,5)P_2 can increase neuronal excitability by modulating ion channels (Zaika et al., 2007).

Fig. 1 represents some of the elements of the PtdIns cycle of synthesis and breakdown as a series of enzymatic and transport steps. We are interested in the subcellular localization and regulation of the lipid 4- and 5-kinase reactions and the regeneration

[1]Department of Physiology and Biophysics, University of Washington School of Medicine, Seattle, WA; [2]Department of Chemistry, University of Washington, Seattle, WA; [3]Department of Brain and Cognitive Sciences, Daegu Gyeongbuk Institute of Science and Technology, Daegu, South Korea.

Correspondence to Bertil Hille: hille@uw.edu.

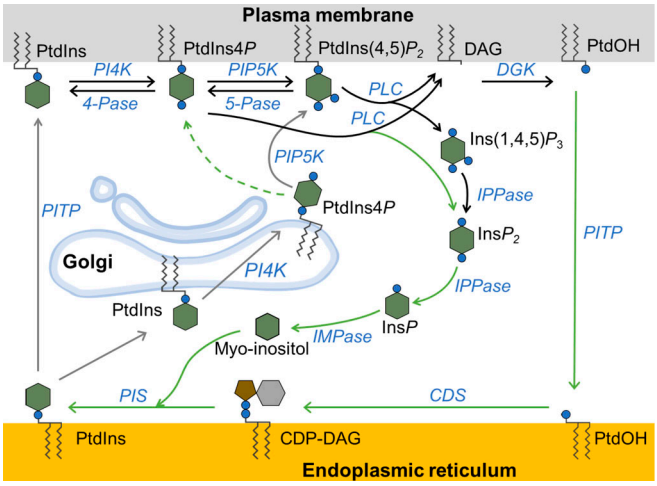

Figure 1. **Schematic of the phosphoinositide cycle in the PM, Golgi, and ER.** Phosphoinositides, lipid phosphatases, and lipid kinases are shown in the PM, ER, and Golgi. Enzymes are shown in blue, fatty acid tails as squiggly lines, inositol as a hexagon, and phosphate as small filled circles. In the PM, PtdIns is phosphorylated by PI4K to PtdIns4*P*, which then is phosphorylated to PtdIns(4,5)P_2 by PIP5K. The phosphatases PtdIns4*P*–4-phosphatase (4-Pase) and PtdIns(4,5)P_2–5-phosphatase (5-Pase) mediate dephosphorylation reactions. Activation of PLCβ hydrolyzes PtdIns(4,5)P_2 to Ins(1,4,5)P_3 and DAG and may also act on PtdIns4*P*. Ins(1,4,5)P_3 is dephosphorylated stepwise, the final step being catalyzed by a lithium-sensitive IMPase. Enzymes in the ER regenerate PtdIns, which can translocate to the PM or Golgi. Golgi PtdIns can be converted to PtdIns4*P*, which in turn goes to the PM to maintain PtdIns(4,5)P_2. Reaction arrows are color-coded according to whether they were included in our first simulation model (black), our second model (black and gray), or neither (green). CDP, cytidine diphosphate; CDS, cytidine diphosphate DAG synthase; DGK, DAG kinase; IPPase, inositol polyphosphate phosphatase; PIS, PtdIns synthase.

of polyphosphorylated inositide pools while they are being depleted by activation of PLC. Many published papers described the depletion of PtdIns(4,5)P_2 during activation of PLC by G_q-coupled receptors such as muscarinic M_1 or angiotensin AT_1 receptors (Kirk et al., 1981; Nakanishi et al., 1994; Willars et al., 1998; Horowitz et al., 2005; Li et al., 2005; Zaika et al., 2006; Bojjireddy et al., 2014; Tóth et al., 2016; Traynor-Kaplan et al., 2017). Our study was motivated by the frequently observed but not yet analyzed finding that if agonist application is maintained, the depleted PtdIns(4,5)P_2 pool slowly starts to grow again (Nakanishi et al., 1994; Li et al., 2005; Zaika et al., 2006; Bojjireddy et al., 2014; Tóth et al., 2016). We reasoned that some aspects of phosphoinositide metabolism must be altered slowly in response to signals generated by agonist action, counteracting the initial lipid depletion. After measuring the muscarinic receptor-induced depletion and regeneration of PtdIns(4,5)P_2 and PtdIns4*P* with optical probes, we tested hypotheses for the mechanisms of lipid regeneration using kinetic simulation in the context of Fig. 1. Of the two principal possibilities, acceleration of lipid kinases versus receptor desensitization with slowing of PLC, we provide strong support and quantitative description for kinase acceleration. Mammalian cells express four types of PI4K enzymes, PI4KIIα, PI4KIIβ, PI4KIIIα, and PI4KIIIβ (Balla et al., 2008). We show that regeneration depends mostly on PI4KIIIα (gene name *PI4KA*). Our analysis also concludes that a significant fraction of the regenerated PM PtdIns(4,5)P_2 is derived from PtdIns4*P* in the Golgi rather than from PtdIns4*P* in the PM.

Materials and methods

Cell culture and gene transfection

All experiments except mass spectrometry used the tsA201 cell line (Sigma) maintained with 5% CO_2 at 37°C in Dulbecco's modified Eagle's medium culture medium (Gibco) supplemented with 10% FBS (Sigma) and 2% penicillin/streptomycin. Cells (passage 15–40) were transfected at ∼75% confluency and subsequently plated on poly-L-lysine–coated coverglass chips (#0; Thomas Scientific). X-tremeGENE 9 (Sigma) and cDNA plasmids were used for transfection.

Plasmids for the pleckstrin homology domain (PH) of PLCδ1 ($PH_{PLC\delta1}$)–CFP and $PH_{PLC\delta1}$-YFP were gifts from Dr. Kees Jalink (van Rheenen et al., 2005); PH_{FAPP}-YFP, OSH-GFP, TGN38–FRB–CFP, and mtq-FAM126A from Dr. Tamas Balla (Balla et al., 2005; Szentpetery et al., 2010); PJ-Sac1–FKBP-mRFP and PJ-dead–FKBP-mRFP from Dr. Gerald R.V. Hammond (Hammond et al., 2012); $Tubby c_{R332H}$-YFP from Dr. Andrew Tinker (Quinn et al., 2008); M_5R, CFP-vector, YFP-vector, CFP-YFP concatemer, C1A-CFP, and C1A-YFP from Dr. Insuk So (Myeong et al., 2015; Myeong et al., 2018); LIBRAvIII from Dr. Akihiko Tanimura (Tanimura et al., 2004); giantin-FRB-CFP from Dr. Takanari Inoue (Komatsu et al., 2010); PI4KIIIα-mcherry, TTC7, and EFR3 from Dr. Pietro De Camilli (Nakatsu et al., 2012); and PI4KIIIβ from Dr. Nicolas Vitale (de Barry et al., 2006). P4M-YFP, Lyn-CFP, and Lyn-YFP were made in the Suh laboratory (Inoue et al., 2005; Keum et al., 2016). M_1R cDNA was purchased from the cDNA Resource Center.

Construction of the Lyn-CFP and Lyn-YFP expression vector

Lyn-CFP and Lyn-YFP were generated by PCR amplification using cDNA of LDR (a kind gift from Takanari Inoue) as a template. A pair of primers was designed: forward 5′-CTTCGA ATTCCGGCCACCATGGGATG-3′ and reverse 5′-CGGTGGATC CGCGCTGTCTTTCC-3′, which contained EcoR1 and HamH1 restriction sites, respectively. The amplified and purified PCR product was ligated into the pGEMT-Easy vector (Promega) to improve the efficiency of ligation of PCR products. The pGEMT-Easy vector containing Lyn insert was digested with EcoR1 and BamH1 (Enzynomics) and ligated with the pECFP-N1 or pEYFP-N1 vector (Clonetech) by T4 DNA ligase (NEB). Lyn-CFP and Lyn-YFP constructs were verified by DNA sequencing (Macrogen) before use.

Fluorescence and three-cube FRET measurements

Three-cube FRET was measured between transfected CFP- and YFP-tagged fluorescent proteins (Erickson et al., 2001). Cells were selected to express about equal amounts of CFP and YFP probes by first measuring the CFP/YFP intensity ratio 0.15–0.21 for a CFP-YFP concatemer (having a guaranteed 1:1 expression) and then using this ratio range as a selection criterion for test cells with a pair of probes. Cells outside the 0.15–0.21 range were rejected. The concatemer with a six-residue spacer between CFP and YFP gave FRET efficiency ($FRET_{eff}$) values of 50–60%.

Excitation light from a TILL monochromator (Polychrome IV) passed into a three-color dichroic mirror cube in an inverted microscope reflecting at 400, 500, and 580 nm (CFP, YFP, and mCherry, respectively; 89006bs; Chroma Technology Corp.) and passing 460–480- and 520–560-nm bands. Emission was collected by a 60× oil objective lens. For FRET, the CFP and YFP emission bands were detected by a TILL photometry system consisting of a TILL ViewFinder to define the rectangular field of measurement, a beam splitter, two photodiodes preceded by ET480/24 (CFP) or ET535/30 (YFP) emission filters, respectively (Chroma Technology Co.), and a TILL FDU-2 detection unit. Recordings were controlled by an EPC9 amplifier with Patchmaster 2.35 software (HEKA). Using the ViewFinder, we could physically acquire a rectangular region of interest for photometry by controlling x- and y-aperture cursors while masking the rest of the field. In a protocol repeated at 1 Hz, Patchmaster collected two signals simultaneously with 440-nm excitation: S_{CFP} (480-nm emission) and S_{FRET} (535-nm emission), followed by one signal with 500-nm excitation: S_{YFP} (535-nm emission). Each photodiode sample was acquired for 20 ms. After recording from one cell was complete, an area of the coverslip without cells was measured as background. The cells were recorded in Ringer's solution containing (in mM) 160 NaCl, 2.5 KCl, 2 $CaCl_2$, 1 $MgCl_2$, 10 HEPES, and 8 glucose and pH 7.4 adjusted with NaOH.

Data were analyzed offline in IGOR Pro 6.37 (WaveMetrics). To calculate $FRET_{eff}$, we needed three constants (R_{D1}, R_{D2}, and R_{A1}) determined before each experiment: $R_{D1} = S_{FRET}(D) / S_{CFP}(D)$, $R_{D2} = S_{YFP}(D) / S_{CFP}(D)$, and $R_{A1} = S_{FRET}(A) / S_{YFP}(A)$, where the notation $S_{cube}(plasmid)$ indicates the intensity S measured with one of three cubes in cells (FRET, CFP, YFP) transfected with D (donor CFP), A (acceptor YFP), or DA (both). They were obtained from measurements with single cells expressing either CFP alone (R_{D1} and R_{D2}) or YFP alone (R_{A1}) and served to remove bleed-through and cross-talk from the signals. With the three constant values, data samples were converted to $FRET_{eff}$ as follows:

$$FRET_{eff} = \left\{ \begin{array}{l} [S_{FRET}(DA) - R_{D1} * S_{CFP}(DA)]/ \\ [R_{A1} * (S_{YFP}(DA) - R_{D2} * S_{CFP}(DA))] - 1 \end{array} \right\} * \{EYFP[440]/ECFP[440]\},$$

where $E_{CFP}(440)$ and $E_{YFP}(440)$ are CFP and YFP molar extinction coefficients.

Estimate of PtdIns(4,5)P_2 concentration using FRET probes

Intermolecular FRET between CFP- and YFP-labeled $PH_{PLC\delta}$ domains was used to estimate the PM PtdIns(4,5)P_2 concentration. The FRET should be proportional to the product of local donor and acceptor concentrations, which in this case are CFP-$PH_{PLC\delta1}$ and YFP-$PH_{PLC\delta1}$ bound to PtdIns(4,5)P_2 at the PM. The product means that FRET should follow a square-law relationship of the number of lipid–probe complexes (Itsuki et al., 2014; Ko et al., 2019b):

$$\frac{FRET_{eff}}{FRET_{eff(max)}} \approx \left\{ \frac{1}{\left[1 + \frac{K_{d(PH)}}{(PtdIns(4,5)P_2)}\right]} \right\}^2, \quad (1)$$

where $K_{d(PH)}$ is the dissociation constant for the complex of $PH_{PLC\delta1}$ with PtdIns(4,5)P_2 (2 µM; Hirose et al., 1999). For calibration, we assumed that the PM density of free PtdIns(4,5)P_2 is 5,000/µm^2 at rest (Falkenburger et al., 2013).

Confocal microscopy

Confocal experiments on live cells were conducted using a Zeiss 710 laser-scanning confocal microscope. Cells were plated on glass-bottom culture dishes (Vita Scientific). Fluorophores were excited by argon (for CFP, GFP, and YFP) and helium-neon (for mCherry or RFP) lasers. The emission was monitored with a 63× oil objective lens. 3-D images of P4M were reconstructed from z-stacks of ∼40 image planes with 0.5-µm spacing. The confocal images were analyzed with ImageJ/Fiji (National Institutes of Health).

Lipid extraction and mass spectrometry

Mass spectrometry was conducted on Chinese hamster ovary (CHO) cells stably transfected with M_1R (from N.J. Buckley and D.A. Brown, University College, London, UK). Previous observations (Horowitz et al., 2005) showed that KCNQ2/3 channel inhibition and $PH_{PLC\delta1}$ translocation to cytoplasm after M_1R activation are identical in CHO cells stably transfected with M_1R and tsA cells (M_1R-transient transfection). These data suggest that the dynamics of PI metabolism are comparable in the two cell lines.

The technique was mostly as published in Traynor-Kaplan et al. (2017). Adherent cells on 35-mm culture dishes (∼1 million cells) were washed twice with Ringer's solution at room temperature. Then, for control cells, ice-cold methanol/1 N HCl was immediately added to stop PtdIns metabolism. For treated groups, methanol/1 N HCl was added after the activation of M_1R for 1 or 10 min with 10 µM oxotremorine-M (Oxo-M). Cells were resuspended with a scraper and collected in an Eppendorf tube. Samples were centrifuged at 12,000 *g* for 3 min at 4°C. Supernatant was discarded, and cells were resuspended in 40 µl ice-cold water. 4 µl of each sample was removed to a different tube for DNA measurements. Then, 10 µl of 6 N HCl, 100 µl butanol, and internal standard (150 ng of 37:4 PtdIns and 20 ng of 37:4 PtdIns4*P* and 37:4 PtdIns(4,5)P_2, from Avanti Polar Lipids) were added to each sample. Samples were vortexed vigorously for 1 min, allowed to sit on ice for 10 min, and centrifuged at 12,000 *g* for 3 min at 4°C. The butanol phase was transferred to a new tube and an additional 100 µl butanol was added to each sample followed by 1 min of vortexing each and centrifugation for 3 min at 12,000 *g*. The new butanol phase was combined with the butanol phase from the first extraction. Then 100 µl chloroform was added to each sample followed by vigorous vortexing and centrifugation at 12,000 *g* for 3 min at 4°C. The chloroform phase was combined with the butanol extract. Two more chloroform extraction steps followed for each sample. Finally, the butanol/chloroform extracts were centrifuged to separate and discard any water phase.

The butanol/chloroform lipid extracts were dried under N_2 (Biotage evaporator) and resuspended in 90 µl methanol/chloroform. Immediately, 20 µl of 2 M trimethylsilyldiazomethane was added to methylate the lipids. The mixture was incubated

for 1 h and applied to an ultra-performance liquid chromatography column coupled to the Xevo TQ-S triple-quadrupole mass spectrometer (Waters Corp). 2 µl of each lipid sample was injected into the port of a C4 column (Waters Acquity UPLC Protein BEH C4; 300A, 1.1 × 100, 1.7 µm). The mobile phase gradient initiated with 10 mM formic acid in water and 10 mM formic acid in acetonitrile, 50%:50% vol/vol increasing to 15%:85%, delivered at a flow rate of 0.1 ml/min. For quantitative analysis, the effluent was monitored in multiple reaction monitoring mode with postcolumn infusion of 50 µM Na formate at 5 µl/min (Traynor-Kaplan et al., 2017). Peak areas of individual lipid species were quantified using QuanLynx software. Peak areas were normalized to the internal standards as (peak area of sample/peak area of standard) * (nanogram of standard) and further corrected to DNA amounts determined with GeneJet Genomic DNAPurification Kit (Thermo Scientific).

Modeling

The kinetics of the PtdIns cycle reactions were modeled by mathematical simulation. The goal was to estimate the time course of key components and the rates of the reaction steps shown in Fig. 1 during long agonist applications as a way to test our hypotheses. The ordinary differential equations of the compartmental model (Falkenburger et al., 2010; Falkenburger et al., 2013) were modified and solved with systematic variations of the parameters using the Virtual Cell environment (University of Connecticut). The rate of each reaction was assumed to be the product of a rate constant times the reactant concentration(s). The Virtual Cell Models "PI cycle 4 & 4S" and "PI cycle figure 6, 7, & S9" by user "Myeong" can be accessed within the VCell software (at https://vcell.org).

Analysis and statistics

The results are presented as mean ± SEM. Statistical significance was determined using the two-tailed Student's *t* test, except Fig. 3 F, Fig. 5, D and E, Fig. S2 B, and Fig. S3 B, which used one-way ANOVA; *, $P < 0.05$ and **, $P < 0.005$. Many FRET values are presented as normalized values (i.e., nFRET). For normalization, the resting FRET value was called 1.0, and zero FRET was called 0.0.

Data availability

All data needed to evaluate the conclusions in the paper are presented in the paper or the supplemental materials.

Online supplemental material

Fig. S1 contains validation of three-cube FRET. Fig. S2 shows that PtdIns(4,5)P_2 regeneration followed initial depletion by receptor stimulation. Fig. S3 compares PtdIns(4,5)P_2 regeneration during stimulation with different muscarinic agonists and receptors. Fig. S4 presents a mathematical model assuming inhibition of phosphatase activities during receptor activation. Fig. S5 shows the intracellular distribution of PI4KIIIα and PI4KIIIβ. Fig. S6 shows localization of PtdIns4*P* at the Golgi and PM. Fig. S7 shows rapamycin-inducible PJ-Sac1 recruitment to the Golgi. Fig. S8 dissects dynamics of phosphoinositide pools with drugs acting on PKC or PI4KIIIα. Fig. S9 shows simulated dynamics of phosphoinositide probes during receptor activation using the expanded mathematical model. Table S1 lists the initial conditions and parameters for the model shown in Fig. 4. Table S2 describes the differential equations for the model shown in Fig. 4. Table S3 lists the initial conditions and parameters for the model shown in Fig. 7 and Fig. S9. Table S4 describes the differential equations for the model shown in Fig. 7 and Fig. S9.

Results

To study the dynamics of the PtdIns cycle and possible adjustments of enzyme rates that may follow activation of receptors, we first measured the reaction steps that are drawn with black arrows in Fig. 1.

Long-term stimulation of G_q-coupled receptors initiates rapid PtdIns(4,5)P_2 depletion followed by gradual regeneration

tsA201 cells were transfected with M_1R muscarinic receptors and stimulated with the muscarinic agonist Oxo-M. We have studied and modeled these kinetics before during brief agonist applications lasting 15–30 s (Falkenburger et al., 2010; Dickson et al., 2013; Falkenburger et al., 2013), but now we studied 10-min agonist applications that engage additional longer-term adjustments of steps in the cycle. We monitored the dynamics of PtdIns(4,5)P_2 using as probes fluorescently labeled PtdIns(4,5)P_2-binding $PH_{PLC\delta1}$ or a YFP-labeled C-terminus of Tubby. Fig. 2 A diagrams the use of $PH_{PLC\delta1}$-CFP and $PH_{PLC\delta1}$-YFP as a FRET pair. When coexpressed in control cells, both of them bind to PtdIns(4,5)P_2 at the PM and have a mutual FRET interaction, but when PtdIns(4,5)P_2 is depleted, they translocate to the cytoplasm where they are too far apart to generate FRET. We call this "homologous FRET" because the CFP and YFP pair each have the same lipid-binding domain. We say "heterologous FRET" when the CFP and YFP pair are attached to different kinds of proteins. To measure the level of PtdIns(4,5)P_2 quantitatively, we used the three-cube method, which reports $FRET_{eff}$ as described previously (Itsuki et al., 2014; Ko et al., 2019b). A control experiment in Fig. S1 showed that cells coexpressing $PH_{PLC\delta1}$-CFP and $PH_{PLC\delta1}$-YFP, which colocalize at the PM, exhibited a robust homologous $FRET_{eff}$ signal, whereas cells coexpressing free cytoplasmic CFP and YFP or the $PH_{PLC\delta1}$-CFP probe and free cytoplasmic YFP showed minimal heterologous $FRET_{eff}$. Thus, this three-cube method greatly reduced bleed-through and cross-talk from fluorescent components that do not interact.

Fig. 2 B shows the biphasic time course of normalized $FRET_{eff}$ ($nFRET_{eff}$) during a 10-min application of agonist. Activation of M_1R by 10 µM Oxo-M promoted the hydrolysis of PtdIns(4,5)P_2, seen as an initial rapid reduction of PH-domain homologous $nFRET_{eff}$ that has been reported many times previously. The key point for this paper, however, is that $nFRET_{eff}$ and therefore the PtdIns(4,5)P_2 level then began to increase again after ∼1 min, despite the continuous presence of the agonist. We will use the word "regeneration" specifically to refer to this slow lipid increment during prolonged receptor activation. We quantified the regeneration in two ways: as regeneration time constant (τ_Regeneration, the red fitted exponential curve of $nFRET_{eff}$ in Fig. 2 B) and as $\Delta nFRET_{eff}$ at 10 min, the difference between the

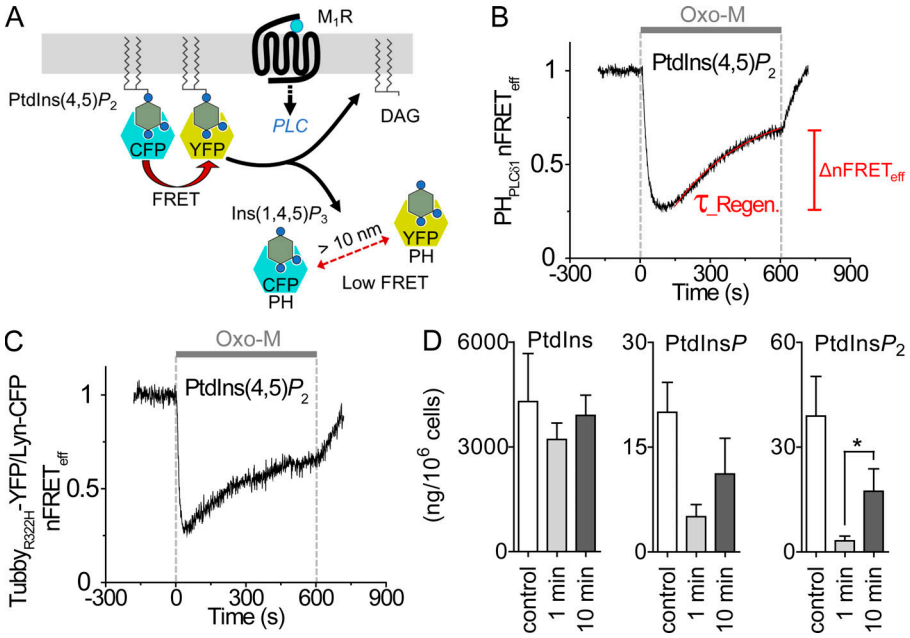

Figure 2. **Depletion and regeneration of PtdIns(4,5)P_2 during stimulation of M_1R. (A)** Schematic of homologous FRET measurements with $PH_{PLC\delta1}$. At the PM, CFP- and YFP-tagged $PH_{PLC\delta1}$ (blue and yellow, respectively) are bound to PtdIns(4,5)P_2 and show a high FRET interaction; however, after the activation of PLCβ, they are released from PtdIns(4,5)P_2 to the cytoplasm and do not generate a FRET signal. **(B)** Time course of PtdIns(4,5)P_2 monitored as the homologous $nFRET_{eff}$ (normalized FRET efficiency) between $PH_{PLC\delta1}$-CFP and $PH_{PLC\delta1}$-YFP in tsA201 cells transfected with M_1R. Activation of M_1R by 10 µM Oxo-M for 10 min (gray bar) depletes PtdIns(4,5)P_2 quickly, but then PtdIns(4,5)P_2 regenerates slowly as fitted with a single-exponential function (red line). $\Delta nFRET_{eff}$ is measured as the difference between the minimal level and the final level at 10 min during Oxo-M stimulation. Here and in the remaining figures, the presented time courses of FRET are representative traces from single cells. **(C)** Time course of PtdIns(4,5)P_2 monitored as the normalized heterologous $FRET_{eff}$ between Lyn-CFP and $Tubby_{R322H}$-YFP. **(D)** Mean of total PtdIns (left), PtdIns$P$ (middle), and PtdInsP_2 (right) in control and 1- or 10-min agonist stimulation measured by mass spectrometry in CHO cells stably expressing M_1R (n = 4 independent lipid extractions). *, P < 0.05.

minimum and the 10-min level. The depth of initial depletion and the $\Delta nFRET_{eff}$ at 10 min were dependent on agonist concentration, but the time constant and the final $nFRET_{eff}$ value at 10 min were not (Fig. S2, A and B). These results were not unique to the agonist Oxo-M or to the specific G_q-coupled receptor. Similar regeneration of PtdIns(4,5)P_2 was seen when carbachol was the agonist instead of Oxo-M (Fig. S3, A and B), and a similar but slower regeneration was seen when the overexpressed receptor was M_5R (Fig. S3, C and D).

Because the $PH_{PLC\delta1}$ probe can bind Ins(1,4,5)P_3 in addition to PtdIns(4,5)P_2 (Hirose et al., 1999), we sought additional verification that PtdIns(4,5)P_2 was regenerating. The first test was to assess PtdIns(4,5)P_2 regeneration using a probe from $Tubby_{R322H}$ (Quinn et al., 2008; Szentpetery et al., 2009), which has a relatively lower affinity for PtdIns(4,5)P_2 than $PH_{PLC\delta1}$ has. We measured $nFRET_{eff}$ between a PM anchor Lyn-CFP and YFP-tagged $Tubby_{R322H}$. This heterologous FRET pair will report PtdIns(4,5)P_2 at the PM more specifically. During long muscarinic stimulation, $Tubby_{R322H}$ showed the expected initial strong $nFRET_{eff}$ decrease followed by regeneration, returning to 0.65 ± 0.06 at 10 min (n = 7; Fig. 2 C). The Tubby results rule out an artifact from a transient rise of Ins(1,4,5)P_3 as the explanation for the transient $PH_{PLC\delta1}$ time course, as well as confirming that regeneration is occurring at the PM.

Second, we used mass spectrometry to measure total cellular polyphosphoinositides (Fig. 2 D). Our technique (Traynor-Kaplan et al., 2017) measured total fatty acyl chain length and the number of phosphates on the inositol head group, but not their position on the inositol ring. To measure changes of phosphoinositide pools during stimulation in a cell population with uniform receptor expression, we used a CHO cell line stably expressing M_1R (n = 4). After 1 min of stimulation with Oxo-M, the total cellular PtdInsP_2 pool showed a sharp reduction, and similar to the results with FRET sensors, at 10 min of stimulation, a significant regeneration (Fig. 2 D). Thus, regeneration involves synthesis and accumulation of new PtdIns(4,5)P_2 and not merely recruitment of PtdIns(4,5)P_2 from one place to another in the cell. The same experiment showed significant depletion and possible regeneration of total cellular PtdIns$P$ during treatment with Oxo-M; however, the 1-min and 10-min points were not statistically distinguishable.

What underlies PtdIns(4,5)P_2 regeneration during long receptor stimulation? We now consider two hypotheses: (i) a secondary acceleration of PtdIns(4,5)P_2 supply due to feedback signals that speed the synthetic enzymes or augment lipid delivery and (ii) a secondary slowing of PtdIns(4,5)P_2 breakdown by PLC, possibly related to desensitization.

Late increase of Ins(1,4,5)P_3 and DAG

As an additional measure of the rate of PtdIns(4,5)P_2 breakdown, we monitored the dynamics of the two PtdIns(4,5)P_2 hydrolysis products, Ins(1,4,5)P_3 and DAG. In principle, the two products should be produced simultaneously and stoichiometrically with PtdIns(4,5)P_2 breakdown, and then they are metabolized independently. Cytoplasmic free Ins(1,4,5)P_3 was estimated using LIBRAvIII (Tanimura et al., 2004), an intramolecular FRET indicator comprising the Ins(1,4,5)P_3 binding domain from an Ins(1,4,5)P_3 receptor sandwiched between CFP and YFP (Fig. 3 A). When Ins(1,4,5)P_3 binds to LIBRAvIII, the distance between CFP and YFP increases and FRET decreases. Therefore, for a

more intuitive presentation, we inverted the $nFRET_{eff}$ axis when plotting LIBRAvIII responses. Although the LIBRAvIII FRET signals have a signal-to-noise ratio that is lower than that of other probes, we continue to present single representative traces as for the other probes. Fig. 3 B shows a rapid transient increase of Ins(1,4,5)P_3 followed by a much slower continued increase during Oxo-M treatment ($nFRET_{eff}$ peak: 0.91 ± 0.01, trough: 0.99 ± 0.01, 5 min: 0.89 ± 0.05, and 10 min: 0.80 ± 0.08; n = 4). Ins(1,4,5)P_3 reached a transient trough 137 s after Oxo-M stimulation. It should be remembered that the expected lifetime of Ins(1,4,5)P_3 is short, 5–30 s (Sims and Allbritton, 1998; Falkenburger et al., 2013), so the instantaneous level of Ins(1,4,5)P_3 would approximately trace its rate of production. Initially, it was produced rapidly as expected, but the rate slowed quickly as the PtdIns(4,5)P_2 substrate was being depleted. Then later, Ins(1,4,5)P_3 production rate steadily increased again, which likely reflects the gradual regeneration of the precursor pool of PM PtdIns(4,5)P_2 (see modeling). There was little FRET change in control cells not expressing M_1R (Fig. 3 B).

For membrane DAG measurement, we used tandem C1A–C1A domains from PKCγ (Fig. 3 A). In resting cells where DAG in the PM is low, the CFP- and YFP-tagged probes were localized in the cytoplasm, producing little FRET (Fig. 3 C). When DAG was increased during receptor activation, the cytoplasmic probes were recruited to the PM and generated a homologous FRET signal that continued to rise until agonist was removed. The expected lifetime of DAG is still relatively short (20–80 s; Suh and Hille, 2006; Falkenburger et al., 2013) but is thought to be longer than for Ins(1,4,5)P_3, so the instantaneous level should almost trace the rate of DAG production but with a longer integration time—effectively more smoothing—than for the LIBRAvIII FRET signal. In a negative-control cell expressing the indicator but no receptor, the $nFRET_{eff}$ signal did not change. The observation of continued rising time courses for Ins(1,4,5)P_3 and DAG will be key for our quantitative dissection of the regeneration mechanism during long agonist application.

Interrupting the phosphoinositide cycle prevents PtdIns(4,5)P_2 regeneration

When receptor-activated PLC depletes PtdIns(4,5)P_2, it also depletes the precursor PtdIns4P (Willars et al., 1998; Horowitz et al., 2005; Balla et al., 2008; Traynor-Kaplan et al., 2017; de Rubio et al., 2018), so subsequent regeneration of PtdIns(4,5)P_2 first requires the synthesis of PtdIns4P from PtdIns by PI4K (Fig. 1). We examined the dependence of PtdIns(4,5)P_2 regeneration on lipid 4-kinases using the broad-spectrum PI4KIII inhibitor wortmannin (Wtn) and the dependence on myo-inositol availability using lithium as an inhibitor of inositol monophosphate phosphatase (IMPase; green arrows in Fig. 1). Low concentrations (0.1 µM) of Wtn strongly inhibit PI3K activity (Hansen et al., 1995), whereas high concentrations (30 µM) also inhibit PI3K, PI4KIIIα, and PI4KIIIβ (Nakanishi et al., 1994; Hansen et al., 1995; Nakanishi et al., 1995; Balla et al., 2008). Fig. 3, D and F, shows that pretreatment of cells with high Wtn (30 µM), which inhibits the three kinases, eliminated the regeneration of PtdIns(4,5)P_2 during long agonist application (purple trace). The plots also show control (gray) and low Wtn pretreatment (0.1 µM; pink) responses for comparison. The strong effect of Wtn here is due to inhibition of type III PI 4-kinases rather than PI 3-kinases.

Lithium inhibits IMPase, the enzyme that restores free myo-inositol pools by dephosphorylating inositol 1-phosphate (Hallcher and Sherman, 1980; Sherman et al., 1985; Berridge et al., 1989) and provides the myo-inositol precursor that is necessary for de novo synthesis of PtdIns (Dai et al., 2016). Fig. 3, E and F, shows that 2-h preincubation with 10 mM lithium also impaired regeneration. In lithium-treated cells, PtdIns(4,5)P_2 regeneration began normally during the first 5 min but then ceased as if the supply of myo-inositol had become exhausted. The PI4KIII inhibitor Wtn similarly decreased the rate of production of the downstream products Ins(1,4,5)P_3 and DAG during agonist application (Fig. 3, G–I). Instead of rising continuously during agonist, Ins(1,4,5)P_3 rose only transiently and DAG rose just to a low steady plateau. Thus, two blockers of the PtdIns cycle suppress the full regeneration of PtdIns(4,5)P_2.

Tests of two hypotheses with a kinetic model

At this point, we had enough information to begin asking about the mechanism for the PtdIns(4,5)P_2 regeneration seen in Fig. 2 B. Could regeneration be due mainly to (i) speeding of production of PtdIns(4,5)P_2 (including speeded delivery of precursors) or to (ii) slowing of breakdown by PLC? To discriminate these alternatives, we turned to kinetic modeling and simulation. We also considered two other minor possibilities. This laboratory has formulated a mathematical model of the enzymatic steps drawn with black arrows in Fig. 1 (Schaff et al., 1997; Falkenburger et al., 2010; Cowan et al., 2012; Falkenburger et al., 2013), a model that was satisfactory to describe the first seconds of receptor activation. The model as drawn (black arrows) places all relevant lipid pools on the PM, a restriction that should not be taken literally and will be corrected later in this paper. With this model as a starting point, we could test the alternative effects of either accelerating the rate of PtdIns(4,5)P_2 synthesis or reducing the rate of PtdIns(4,5)P_2 breakdown during longer receptor activation. To match our observations, either of these changes would need to develop slowly (over several minutes) after agonist application. The values assumed for fixed kinetic constants, initial conditions, and reaction kinetics are summarized in Table S1 and Table S2. They are mostly taken directly from our previous modeling (Falkenburger et al., 2010; Falkenburger et al., 2013).

For the first manipulation, instead of leaving the PI4K activity invariant in the model after the first seconds of receptor activation, we tested hypothetical secondary gradual rate increases represented in Fig. 4 A. As in the Falkenburger model, the rate constant for PI4K is quickly stepped up 10-fold in the first second after agonist application, but now it continues to grow gradually by another large factor (with an exponential time constant of 300 s). As anticipated, with these slow secondary increases of PI4K activity, the simulated PtdIns4P (Fig. 4 B) and PtdIns(4,5)P_2 (Fig. 4 C) showed gradual regeneration, and, as in the experiments of Fig. 3, Ins(1,4,5)P_3 increased transiently followed by a secondary slow increase (Fig. 4 D), and DAG showed a fast initial increase and then a slow steady rise

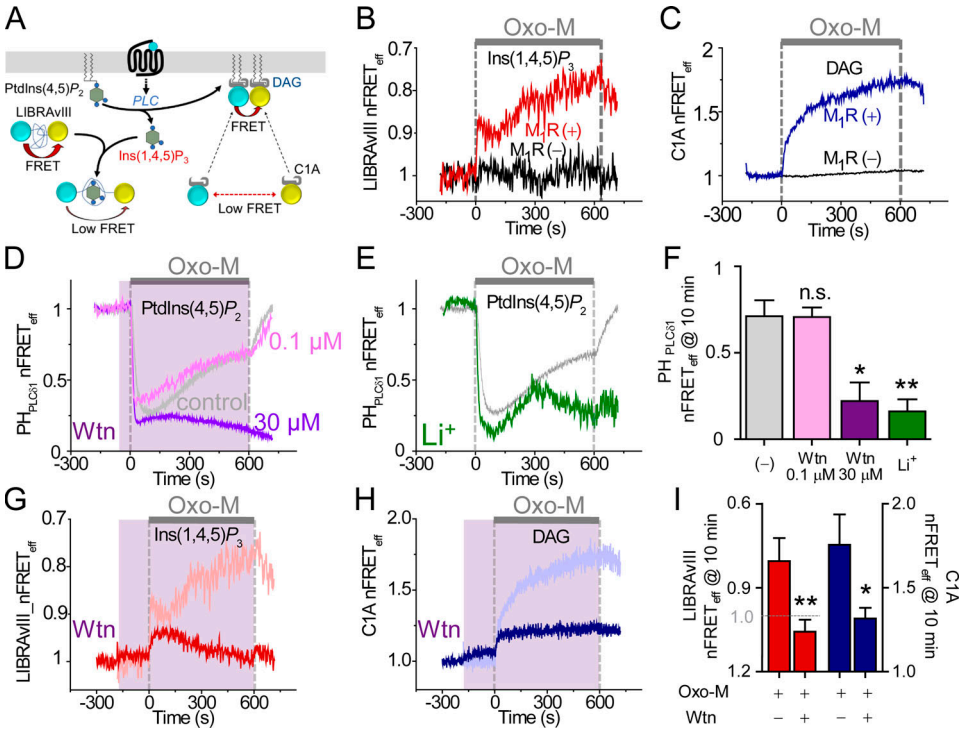

Figure 3. **Exploring steps of the PI cycle by monitoring Ins(1,4,5)P_3, DAG, and PtdIns(4,5)P_2. (A)** Schematic of Ins(1,4,5)P_3 and DAG indicators. LIBRAvIII has CFP and YFP at opposite termini of an Ins(1,4,5)P_3 binding domain. **(B)** Time course of intramolecular LIBRAvIII nFRET$_{eff}$ during a 10-min stimulation with 10 µM Oxo-M (gray bar) in cells with or without expression of M_1R. Note inverted y axis for LIBRAvIII since FRET is reduced by binding of Ins(1,4,5)P_3 to this receptor. **(C)** Time course of homologous nFRET$_{eff}$ between CFP- and YFP-tagged C1A domains with or without expression of M_1R. CFP- and YFP-tagged C1A domains detect DAG at the PM and increase their FRET when DAG increases at the PM. **(D)** Comparison of pretreatment with 0.1 µM or 30 µM Wtn (shaded area) on PtdIns(4,5)P_2 regeneration during M_1R stimulation by 10 µM Oxo-M (gray, control; pink, 0.1 µM Wtn; and purple, 30 µM Wtn). **(E)** Effect of 2-h pretreatment with 10 mM Li^+-enriched solution on regeneration of PtdIns(4,5)P_2 (gray, control; green, Li^+). **(F)** Mean PtdIns(4,5)P_2 regeneration measured as homologous nFRET$_{eff}$ of CFP- and YFP-tagged PH$_{PLC\delta1}$ at 10 min of Oxo-M treatment. Control, n = 6 cells; 0.1 µM Wtn, n = 9; 30 µM Wtn, n = 9; Li^+, n = 4. **(G)** Wtn (shaded area) limits Ins(1,4,5)P_3 regeneration during M_1R activation as measured with LIBRAvIII (pink, control; red: 30 µM Wtn). **(H)** Wtn depresses DAG production as measured with C1A probes (aqua, control; blue, 30 µM Wtn). **(I)** Mean Wtn effect on production of Ins(1,4,5)P_3 (red bars) and DAG (blue bars) measured as nFRET$_{eff}$ at 10 min of Oxo-M treatment. Ins(1,4,5)P_3: control, n = 4 cells and Wtn, n = 6; DAG: control, n = 9 and Wtn, n = 6 cells. *, P < 0.05; **, P < 0.005. n.s., not significant.

(Fig. 4 E). In the calculations, the black curves resemble the experiments enough to suggest that such a model could be a satisfactory beginning. At the end of 10 min, the PI4K activity had risen to 100× its resting value. These two ad hoc phases of PI4K increase would have to be a consequence of receptor activation.

One might also ask whether increasing PIP5K alone instead of PI4K alone might do equally well. This possibility was tested in Fig. 4, F–J. However, it did not work well even if we accelerated PIP5K activity by 100-fold. Basically, as PIP5K was accelerated, it depleted the pool of PtdIns4P toward zero so that the supply of PtdIns(4,5)P_2 became entirely limited by the constant ability of PI4K to supply more PtdIns4P for conversion to PtdIns(4,5)P. Thus, speeding PIP5K was not sufficient by itself; it would have to be accompanied by speeding of PI4K to work.

To test the main alternative hypothesis, which postulated a gradual slowing of PtdIns(4,5)P_2 breakdown, we tried a slow secondary decay of PLC activity (Fig. 4 K). Such a change might represent receptor desensitization. As anticipated, the simulated PtdIns(4,5)P_2 level did show good rebound during the strongest gradual slowing of PLC activity (Fig. 4 M). However, while PLC was slowed eventually by 85%, the simulated time courses of Ins(1,4,5)P_3 and DAG production showed only an initial step-up but no subsequent growth (Fig. 4, N and O), unlike the observations in Fig. 3, B and C. There simply was insufficient ongoing breakdown of PtdIns(4,5)P_2 when PLC was slowed. Therefore, our modeling suggests that a slow speeding of PtdIns(4,5)P_2 synthesis or supply could be the dominant contributor to PtdIns(4,5)P_2 regeneration during M_1R stimulation.

One might suppose that regeneration could also be mimicked by a slow profound inhibition of lipid phosphatases. However, this idea fails entirely because in the Falkenburger model the PI4K and PIP5K activities are stepped up 10-fold already in the first second of receptor activation, leaving the 4- and 5-phosphatase activities already very small by comparison. Further gradual slowing of the phosphatase activities to zero had little effect on the predicted PtdIns4P, PM PtdIns(4,5)P_2, Ins(1,4,5)P_3, and DAG (Fig. S4, A–F), although magnifying the simulated traces sufficiently did reveal a very tiny effect in the expected direction (Fig. S4, C–F, lower panels).

PI4KIIIα contributes to PtdIns(4,5)P_2 regeneration during receptor stimulation

The simulations focused our attention on the PI4K enzymes. Which PI4K subtypes are involved? Where are they located?

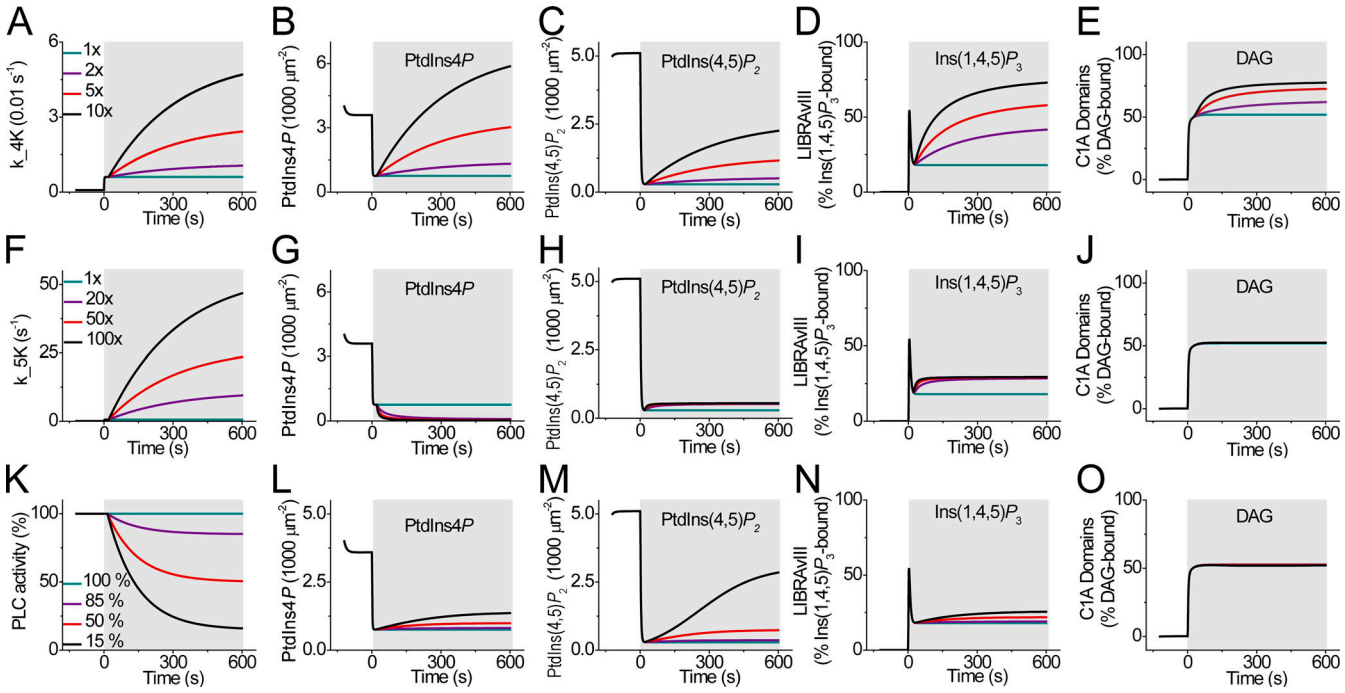

Figure 4. **Three modified mathematical models simulating PtdIns(4,5)P_2 regeneration during receptor activation.** All curves are simulations with receptor activation during the shaded areas. **(A–O)** Comparison of the assumption of PI4K acceleration (A–E), PIP5K acceleration (F–J), or PLC desensitization (K–O) as explanations of PtdIns(4,5)P_2 regeneration. All models consider only the steps with black arrows in Fig. 1, and they assume that the concentration of PtdIns at the PM remains constant. **(A, F, and K)** Panels show the range of hypothetical time courses tested for the kinetics of PI4K, PI5K, or PLC, respectively. They are evaluated by the simulations in the four panels to the right of them. **(A–E)** Progressive acceleration of PI4K during 10-µM Oxo-M stimulation. **(A)** Assumed accelerations of the rate of PI4K in the first model during M_1R activation, ranging from the standard Falkenburger model (green curve) to increasing accelerations (violet, red, and black). **(B–E)** The predicted concentrations of PM PtdIns4*P* (B) and PtdIns(4,5)P_2 (C), Ins(1,4,5)P_3 interacting with LIBRAvIII (D), and DAG interacting with C1A domains (E), color-coded as in A. **(F–J)** Progressive acceleration of PIP5K during 10-µM Oxo-M stimulation, shown in the same format as A–E. **(K–O)** Progressive slowing of PLC activity during 10-µM Oxo-M stimulation.

Where are the pools of PtdIns4*P* that they make? Does this affect the simulations? In general, PI4KIIIα has been recognized as the principal 4-kinase supplying PM PtdIns(4,5)P_2 by pharmacology (Balla et al., 2008) and by knockout approaches (Nakatsu et al., 2012). We took the pharmacological approach using PI4K inhibitors with the different reported selectivities listed in Fig. 5 A (Bojjireddy et al., 2014; Tóth et al., 2016). Pretreatment with phenylarsine oxide (PAO), Wtn, or A1 abolished PtdIns(4,5)P_2 regeneration during M_1R activation, whereas PIK93 did not (Fig. 5, B and D). By elimination, the block by A1 and not by PIK93 left PI4KIIIα as the principal 4-kinase relevant for PtdIns(4,5)P_2 regeneration.

In a similar protocol, we measured the time course of PtdIns4*P* at the PM. We monitored heterologous FRET between CFP-tagged P4M, a PtdIns4*P* probe (Hammond et al., 2014), and PM-anchored Lyn-YFP, comparing the different inhibitors of PI4K. This FRET measurement is restricted to the PM where Lyn is localized. Strikingly, the simple addition of PAO, Wtn, or A1 (but not PIK93) initiated an immediate gradual decline in the PM PtdIns4*P* signal at a rate of ∼5%/min (Fig. 5 C). This pattern of decline implied that the resting PM PtdIns4*P* is maintained primarily by continuous action of PI4KIIIα and not by PI4KIIIβ. After 3 min in the inhibitor or without inhibitor (control), PLC was activated with Oxo-M. In control, the expected sharp drop in PtdIns4*P* quickly reached a plateau with perhaps a slight slow rise resembling regeneration. Quite unlike for PM PtdIns(4,5)P_2, the small regeneration of PM PtdIns4*P* was sensitive only to PAO pretreatment and not to the other PI4K inhibitors (Fig. 5, C and E). Indeed, with PAO, Oxo-M depressed PtdIns4*P* well below the plateau seen in the control or with the other inhibitors. The insensitivity of PM PtdIns4*P* to Wtn, A1, and PIK93 during receptor activation suggests that the principal precursor for A1-sensitive PtdIns(4,5)P_2 regeneration during challenge by prolonged M_1R stimulation is not this pool of PtdIns4*P* at the PM, so we considered other sources.

Golgi PtdIns4*P* contributes to PtdIns(4,5)P_2 regeneration

Confocal microscopy with overexpressed fluorescent 4-kinases coexpressed with the auxiliary proteins EFR3 and TTC7 with or without the complexing protein FAM126A showed that, in tsA201 cells, PI4KIIIα fluorescence overlapped both the trans-Golgi region and the cell surface, as did FAM126A (Fig. S5, A and B), whereas PI4KIIIβ fluorescence overlapped primarily the Golgi (Fig. S5 C). Previously, we showed that PtdIns4*P* pools in both the Golgi and the PM support PtdIns(4,5)P_2 synthesis at the PM, which is needed for PM ion channel function (Dickson et al., 2014). Using 3-D confocal images (z-stacks) of the PtdIns4*P* probe P4M-CFP, we now estimated by integration of intensities in every section that approximately half of cellular P4M-CFP fluorescence is in the Golgi region and half is near the PM (Fig.

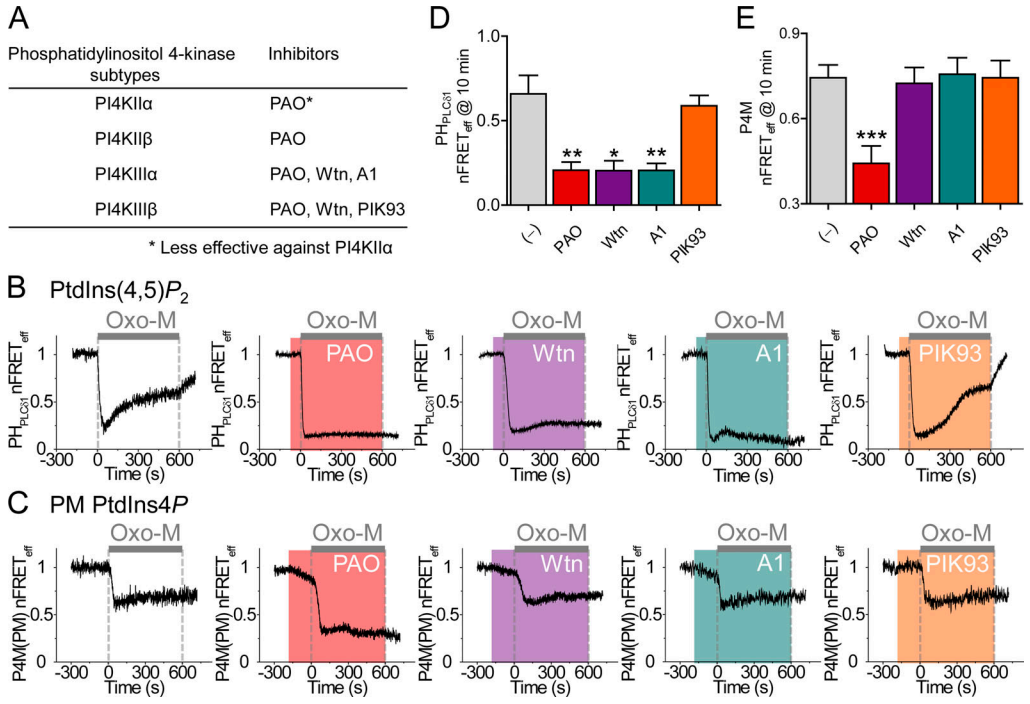

Figure 5. **Depression of PtdIns(4,5)P_2 regeneration by PI4KIIIα inhibitors. (A)** Specificity of inhibitors for PI4K subtypes. **(B)** Time course of PtdIns(4,5)P_2 during 10-µM Oxo-M application (gray bar) measured from homologous FRET between CFP- and YFP-tagged $PH_{PLC\delta1}$ probes in cells pretreated (shaded areas) with different PI4K inhibitors (30 µM PAO, 30 µM Wtn, 30 nM A1, and 300 nM PIK93). **(C)** Time course of PtdIns4*P* in the PM measured from heterologous FRET between P4M-CFP and Lyn-YFP in cells pretreated (shaded areas) with different PI4K inhibitors. **(C–E)** Mean PI4K inhibitor effects on the regeneration of PtdIns(4,5)P_2 (D) and on PM PtdIns4*P* (E) as measured with FRET indicators at 10 min of Oxo-M stimulation. PtdIns(4,5)P_2: control, n = 4 cells; PAO, n = 5; Wtn, n = 5; A1, n = 8; and PIK93, n = 9. PtdIns4*P*: control, n = 25; PAO, n = 15; Wtn, n = 15; A1, n = 12; and PIK93, n = 7 cells. *, P < 0.05; **, P < 0.005; ***, P < 0.001.

S6). We measured the time course of depletion of the Golgi PtdIns4*P* pool during M_1R stimulation using a YFP-tagged PH domain of FAPP1 (PH_{FAPP1}; Fig. 6 A). This probe is considered to report trans-Golgi PtdIns4*P* but not PM PtdIns4*P* (Hammond et al., 2014; Liu et al., 2014). The confocal images in Fig. 6 A support this selectivity. When Oxo-M was applied, the Golgi PH_{FAPP1} intensity decreased monotonically, giving no hint of regeneration in this Golgi pool during receptor activation (Fig. 6 A). In parallel experiments, we measured PtdIns(4,5)P_2 at the PM with homologous normalized FRET between CFP- and YFP-tagged $PH_{PLC\delta1}$ to calculate quantitative PtdIns(4,5)P_2 density by (Fig. 6 B). The quantitative estimation involved a nonlinear transform explained in the Materials and methods (Eq. 1). The time constant for PtdIns(4,5)P_2 regeneration at the PM was about the same as that for the reduction of PtdIns4*P* in the trans-Golgi (Fig. 6 C), as might be the case, for example, if Golgi PtdIns4*P* were the key source tapped for regeneration of PM PtdIns(4,5)P_2. We note that a quite similar but more modest monotonic falling time course of Golgi PH_{FAPP1} labeling was reported in several cell lines during 30-min application of 100 nM endothelin-1 (de Rubio et al., 2018); however, that paper interpreted the fall as being due to direct hydrolysis of PtdIns4*P* by PLC in the Golgi rather than due to depletion by transfer to the PM.

To explore the contribution of Golgi PtdIns4*P* to regeneration of PtdIns(4,5)P_2, we depleted Golgi PtdIns4*P* by a rapamycin-induced heterodimerization system. A PtdIns4*P* 4-phosphatase (PJ-Sac1; Hammond et al., 2012) fused with FK506-binding protein (FKBP) was recruited to the Golgi anchor, giantin, fused with an FKBP-rapamycin binding (FRB) domain (Fig. S7 A; Choi et al., 1996; Liang et al., 2014). There, the recruited phosphatase converted Golgi PtdIns4*P* to PtdIns (Fig. S7 B; Dickson et al., 2014). In control experiments where an enzymatically inactive phosphatase (PJ-dead) was recruited to the Golgi, PtdIns(4,5)P_2 regenerated normally during prolonged M_1R receptor activation (Fig. 6 D). However, if an active PJ-Sac1 was recruited to the Golgi-localized giantin 60 s before receptor stimulation, the later phase of the PM PtdIns(4,5)P_2 regeneration was eliminated (Fig. 6 D; PJ-Dead: 0.67 ± 0.11 $nFRET_{eff}$ at 10 min [n = 5]; PJ-Sac1: 0.32 ± 0.04 $nFRET_{eff}$ at 10 min [P = 0.003; n = 5]). Thus, the Golgi PtdIns4*P* pool makes a rapid and essential contribution to PtdIns(4,5)P_2 regeneration at the PM during receptor activation. Possibly, the early transient of regeneration with PJ-Sac reflects some initial regeneration of PtdIns(4,5)P_2 from a small, rapidly depleting pool of PtdIns4*P* at the PM.

Similar experiments attempted to use P4M probes and Lyn-YFP to monitor PM PtdIns4*P*, while PJ-dead or PJ-Sac1 was recruited to the Golgi (Fig. 6 E). The control PJ-dead experiment preserved the typical decrease and weak apparent regeneration of PM PtdIns4*P*. But the PJ-Sac1 recruitment experiment showed an unanticipated initial rise of the PM P4M probe signal with rapamycin before Oxo-M was applied, followed by the expected decrease with Oxo-M and again a small apparent regeneration (Fig. 6 E). Modeling shown later explained the initial rise and the

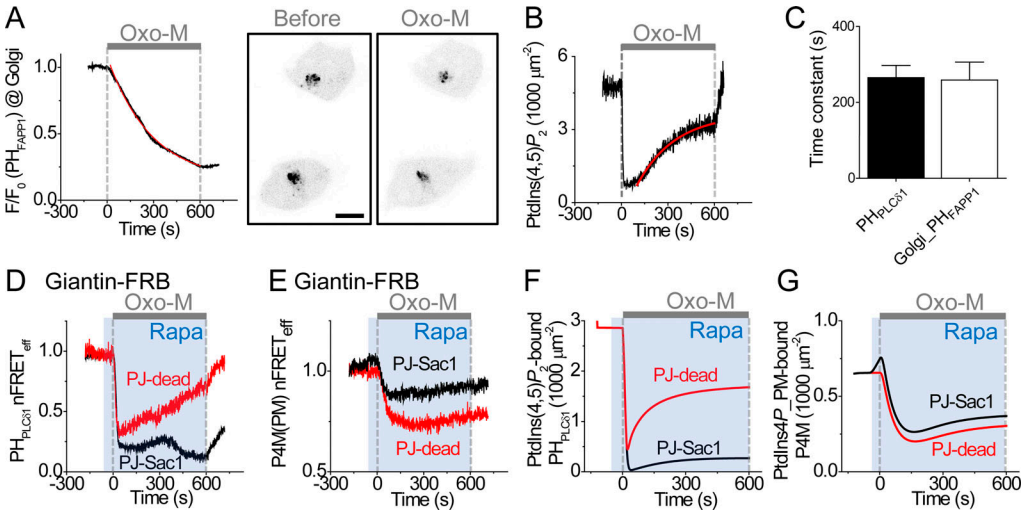

Figure 6. **Participation of Golgi PtdIns4*P* in the regeneration of PM PtdIns(4,5)P_2 during M_1R activation. (A)** Left: Time course of Golgi PtdIns4*P* level during M_1R stimulation measured with photometry of PH_{FAPP1}-YFP, a probe specific for Golgi PtdIns4*P*. The fluorescence signal normalized to the initial fluorescence (F/F_0) was fitted by a single exponential function (red line). Confocal images of PH_{FAPP1}-YFP on the right side show reduction of Golgi PtdIns4*P* after M_1R activation for 10 min. Scale bar, 10 µm. Different experiment from the photometry time course on the left. **(B)** Time course of PtdIns(4,5)P_2 concentration (density) during application of Oxo-M (gray bar) calculated from homologous $FRET_{eff}$ of CFP- and YFP-tagged $PH_{PLC\delta1}$ probes using Eq. 1. Regeneration of PtdIns(4,5)P_2 was fitted with a single exponential curve (red line). **(C)** Mean time constants decrease for Golgi PtdIns4*P* (n = 3 cells) and increase for PM PtdIns(4,5)P_2 (n = 8 cells). **(D)** Depression of PtdIns(4,5)P_2 regeneration by Golgi recruitment of PJ-Sac1 phosphatase or PJ-dead with 1 µM rapamycin (blue shading, Rapa). $nFRET_{eff}$ between CFP- and YFP-tagged $PH_{PLC\delta1}$ domains measured during 10 µM Oxo-M (gray bar). **(E)** Comparison of PJ-Sac1 or PJ-dead recruitment to the Golgi by 1 µM rapamycin PM on PtdIns4*P* regeneration during receptor activation. $nFRET_{eff}$ between P4M-CFP and Lyn-YFP measured during application of rapamycin followed by 10 µM Oxo-M. **(F and G)** Simulation of PtdIns(4,5)P_2 regeneration (F) and PtdIns4*P* regeneration (G) during Golgi action of PJ-Sac1 and PJ-dead using the expanded model also used for Fig. 7 and Fig. S9.

late apparent regeneration as artifacts. Both rises were caused by the large gradual release of the P4M probe from the Golgi, while PJ-Sac1 and PLC action depleted the PtdIns4*P* pool there (measured in Fig. 6 A). Essentially, P4M probes would be transferred gradually from declining PtdIns4*P* pools on Golgi membranes to the PM, even if PtdIns4*P* were constant at the PM. Successful modeling (shown in Fig. 6 G) showed that the evoked intermembrane transfer of P4M probes considerably distorted the experimentally recorded FRET signal. In this case, modeling proved essential to validate our interpretation of an artifact. A similar intermembrane transfer of GFP-P4M-P4M probes but in the opposite direction was reported when PM PtdIns4*P* was depleted by neurotensin receptor activation, and P4M-P4M probe labeling in the Golgi increased (de Rubio et al., 2018). Such transfers can happen whenever a diffusible probe can label two pools in the cell that have very different temporal dynamics.

Is acceleration of kinases due to DAG and PKC?

Our attention was drawn to observations by Tóth et al. (2016) of significant slow elevations of PM PtdIns4*P* when cells were stimulated very mildly with only 100 nM carbachol or 17 nM epidermal growth factor. We could duplicate these observations using 10 nM Oxo-M (Fig. S8 A). This slow elevation of PtdIns4*P* contrasts with the sharp decrease seen with 10 µM Oxo-M (Fig. 5 C) and with the lack of effect of 10 nM Oxo-M in PM PtdIns(4,5)P_2 (Fig. S2). Further, Tóth et al. (2016) gave evidence that the secondary increase of PM PtdIns4*P* was due to DAG-dependent activation of PKC, and we could duplicate these observations, finding that the rise with 10 nM Oxo-M was partly blocked by 2 µM bisindolylmaleimide I (BIM), a PKC inhibitor (Fig. S8 A), and was mimicked by 5 µM PMA, a PKC activator (Fig. S8 B). The slow PtdIns4*P* rise during the low 10-nM Oxo-M stimulation was reminiscent of the slow regeneration of PtdIns(4,5)P_2 that we saw with high agonist concentrations (Fig. 2 B). Did DAG and PKC also contribute to regeneration during this much stronger receptor stimulation? We have seen that DAG itself rises in two phases, an initial transient followed by a secondary slow rise (Fig. 3 C). Hence, it could be possible that DAG is a diphasic signal that through PKC leads to two cumulative stages of activation of lipid kinases during strong receptor stimulation. Unfortunately for this hypothesis, we found that PM PtdIns4*P* continued to increase during 10-nM Oxo-M stimulation (low agonist concentration) and during 5-µM PMA stimulation, even when the A1 inhibitor was used to block PI4KIIIα (Fig. S8, B and C); additionally, BIM was unable to inhibit regeneration of PtdIns(4,5)P_2 at high agonist concentration (Fig. S8 D).

Exploring a kinetic model with Golgi and ER compartments

Another round of refinement of the kinetic model helped us develop a better understanding of the contribution of intracellular organelles to PtdIns(4,5)P_2 regeneration. We augmented the previous model by simulating added Golgi pools of PtdIns and PtdIns4*P* and an ER pool of PtdIns plus additional catalyzed steps represented as gray arrows in Fig. 1. One gray arrow labeled phosphatidylinositol transfer protein (PITP) represents transfer of PtdIns from the ER to the PM by transfer proteins (Kim et al., 2015; Pemberton et al., 2020). Another, labeled

PIP5K from Golgi PtdIns4*P* to PM PtdIns(4,5)P_2, represents transfer of PtdIns4*P* from the Golgi to the PM accompanied by simultaneous phosphorylation by a 5-kinase, an unconventional lumped reaction that we gave evidence for before (Dickson et al., 2014). To make regeneration of PM PtdIns4*P* independent from Golgi PtdIns4*P*, the calculations omit a direct Golgi PtdIns4*P* contribution to PM PtdIns4*P*, the dashed green line in Fig. 1. The values assumed for fixed kinetic constants, initial conditions, and reaction kinetics in this refined model are summarized in Table S3 and Table S4. The revised simulation, now including both black and gray arrows of Fig. 1, again has the activity of the PI4K enzyme slowly increasing during receptor stimulation now both in the Golgi and in the PM, as plotted in Fig. 7, A and B. The time-dependent activities stepped up quickly initially (at the PM but not for the Golgi) and then increased monotonically with a time constant of 300 s after agonist application. In accord with recent reports that PtdIns is nearly absent from the PM in resting cells (Pemberton et al., 2020; Zewe et al., 2020), the revised model assumed a 1:50:50 (PM:Golgi:ER) basal distribution of PtdIns. And since previous work and our Fig. 2 D reported as little as 10% change of total cellular PtdIns during receptor stimulation (Willars et al., 1998; Horowitz et al., 2005; Traynor-Kaplan et al., 2017), for simplicity the revised model kept the PtdIns of the ER at a constant value and did not represent its synthesis—omitting any green arrows in Fig. 1. PtdIns of the PM and the Golgi was allowed to vary. Pemberton et al. (2020) showed a small (1%) transient increase of PM PtdIns during strong activation of angiotensin II receptors, so we also added a small, slow increase of PITP activity from the ER to the PM (τ = 100 s). In a study similar to ours, Nir2, a PITP, translocated to the PM from the ER during stimulation with a ∼1-min time constant (Chang and Liou, 2015).

We simulated time courses of the actual lipid and product molecules (Fig. 7) as well as time courses of the substrate-bound indicator probes for easier comparison with the experimental traces (Fig. S9). The model gave the following results during receptor stimulation: (i) a biphasic change of PM PtdIns (Fig. 7 C); (ii) a monotonic fall of Golgi PtdIns (Fig. 7 D); (iii) biphasic dynamics of PM Ptdins4*P* (Fig. 7 E and Fig. S9 A); (iv) a monotonic fall of Golgi PtdIns4*P* (Fig. 7 F and Fig. S9 B); (v) a fast loss and slow regeneration of PM PtdIns(4,5)P_2 (Fig. 7 G and Fig. S9 C); (vi) both a transient and a secondary increase of Ins(1,4,5)P_3 (Fig. 7 H and Fig. S9 D); and (vii), a rapid initial and slow further increase of DAG (Fig. 7 I and Fig. S9 E). Most of the PtdIns(4,5)P_2 was generated by the lumped transport/5-kinase reaction, depleting the Golgi pool of PtdIns4*P* faster than it could be synthesized from Golgi PtdIns. The time course of PtdIns4*P* is shown as regenerating very modestly at the PM and depleting in the Golgi (Fig. 7, E and F). These simulations recapitulate key features of our experimental results (Fig. 2, Fig. 3, Fig. 5, and Fig. 6), supporting time-dependent contributions of Golgi PI4K and Golgi PtdIns4*P* to the regeneration of PM PtdIns(4,5)P_2 during receptor and G_q stimulation. Adding recruitment of Sac1 to the Golgi in the model showed reduced PtdIns(4,5)P_2 regeneration (Fig. 6 F) and a transient increase followed by biphasic loss and overshooting rise of the PtdIns4*P* reporter P4M (Fig. 6 G). Thus, the simulated kinetics recapitulated the experimental results satisfactorily.

Discussion

This study measured the real-time kinetics of phosphoinositides during long activation of M_1 muscarinic receptors. We studied PtdIns(4,5)P_2, PtdIns4*P*, and DAG in the PM, PtdIns4*P* in the Golgi, and Ins(1,4,5)P_3 in the cytoplasm. Our focus was on the regeneration of PtdIns(4,5)P_2, and the key new approach was to use quantitative interpretations of the results to test hypotheses. In many respects, we support and extend earlier observations concerning (i) receptor-induced acceleration of PtdIns(4,5)P_2 synthesis, (ii) the importance of PI4KIIIα as the enzyme to regenerate PM PtdIns(4,5)P_2, and (iii) a contribution of PtdIns4*P* from the Golgi to PM PtdIns(4,5)P_2. We now compare our results with the literature and expand our interpretations.

Regeneration of PtdIns(4,5)P_2 by acceleration of lipid kinases

We have highlighted PtdIns(4,5)P_2 regeneration, a refilling of the PM PtdIns(4,5)P_2 pool(s) during prolonged activation of M_1R and M_5R. Although it has not received much analysis before, quite similar regeneration seems evident in published figures showing chemical analyses of phosphoinositides during receptor activation (Nakanishi et al., 1994; Li et al., 2005; Zaika et al., 2006) and in experiments with $PH_{PLC\delta1}$ probes (Tóth et al., 2016; Ko et al., 2019a; Pemberton et al., 2020). These published experiments used muscarinic and angiotensin II receptors, suggesting that regeneration is not confined to muscarinic receptors. Likely, regeneration in the earlier records did not attract much attention since it would also happen if the receptors had undergone desensitization. In other experiments using known rapidly desensitizing receptors such as the bradykinin receptor or protease activated receptor 2, PtdIns(4,5)P_2 recovered even sooner during agonist application (Xu et al., 2003; Jung et al., 2016), but there, it was clear that lipid breakdown had been arrested quickly by rapid and profound receptor desensitization.

Without simultaneous tests for desensitization or for large continued Ins(1,4,5)P_3 and DAG production, it would be hard to interpret many isolated records in the literature. Compared with, for example, α_{1B} adrenergic receptors, M_1 muscarinic receptors are slow to desensitize (Kienitz et al., 2016). We have found before that although M_1 muscarinic receptors do bind β-arrestin-2 to ∼50% occupancy, they are not internalized during a 10-min stimulation (Jung et al., 2017). In our modeling, PtdIns(4,5)P_2 regeneration with continued DAG and Ins(1,4,5)P_3 production during Oxo-M application could not be explained by slowing PLC (desensitization), but instead required a gradual acceleration of lipid kinase activity. Simulation trials with desensitization of only 50% (starting with overexpressed levels) failed to mimic any regeneration (Fig. 4 M) and, with much stronger desensitization, did show PtdIns(4,5)P_2 regeneration but failed to produce accelerating accumulation of Ins(1,4,5)P_3 and DAG over 10 min (Fig. 4, N and O). Angiotensin II receptors are also said to desensitize weakly. AT_1R has 12 serine/threonine potential phosphorylation sites in the C terminus compared with three in the M_1 receptor. Protease activated receptor 2 has 17. In

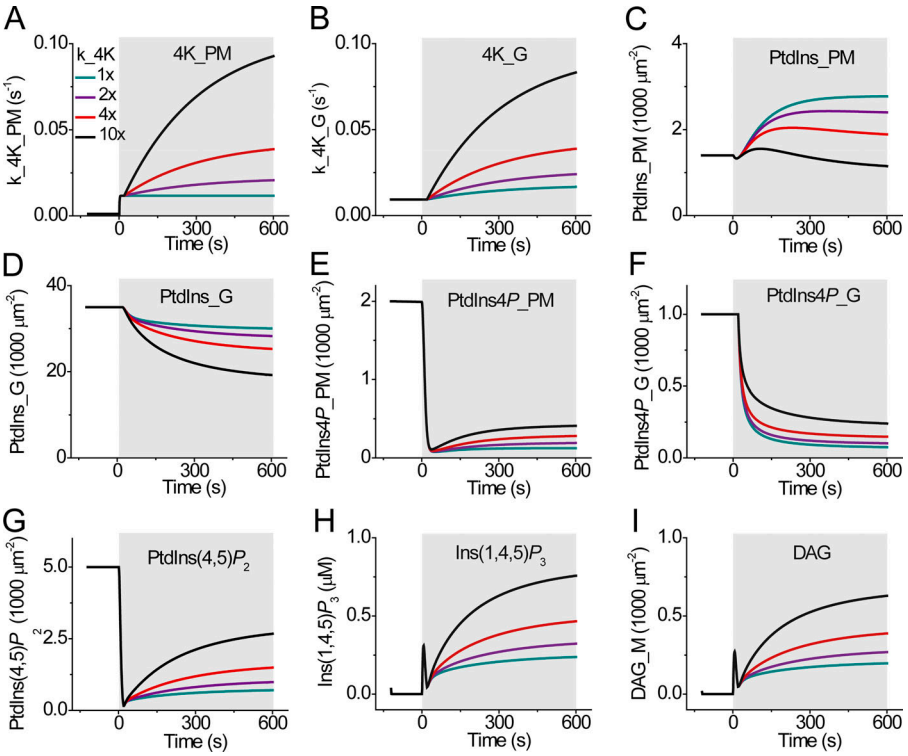

Figure 7. **Expanded mathematical model with the additional contribution of Golgi PtdIns4*P*. (A–I)** Calculations from an expanded model to include the gray arrows as well as the black arrows of Fig. 1. Several time-varying changes were assumed and tested for the rate constants for PI4K of the PM (A) and of the Golgi (B) during Oxo-M (shaded area). Corresponding simulated time courses of PM PtdIns (C), Golgi PtdIns (D), PM PtdIns4*P* (E), Golgi PtdIns4*P* (F), PM PtdIns(4,5)P_2 (G), Ins(1,4,5)P_3 (H), and PM DAG (I). The concentration of PtdIns at the ER is held constant. _G indicates chemical species in the Golgi compartment.

5 min of angiotensin II exposure, phosphorylation of AT_1 receptors only doubles over the resting level, and only 20% of the receptors internalize (Bojjireddy et al., 2015). In the future, it would be nice to see more studies of 10-min applications of angiotensin II combined with some of the more direct functional measures used here and a more quantitative kinetic analysis.

The idea of kinase acceleration upon agonist addition is not new. It was postulated in earlier models of phosphoinositide metabolism. An early model invoked almost immediate 3.5-fold and 19-fold steady increases of PI4K and PIP5K activity, respectively (Xu et al., 2003). This explained a short transient increase of PtdIns(4,5)P_2 that preceded a rapid decrease of PtdIns(4,5)P_2 during bradykinin application. Similarly, Falkenburger et al. (2013) postulated quick, 10-fold increases of both kinases to explain continued generation of Ins(1,4,5)P_3 during 3-min M_1 receptor activations. In the latter model, the acceleration of kinases developed within <1 s whenever the Oxo-M concentration was above ∼20 nM. New in our analysis of regeneration is that the early kinase acceleration of the Falkenburger model, though essential, was insufficient to mimic longer agonist applications. We required considerable secondary acceleration of PI4K activity that had to develop slowly—over several minutes—to describe the gradual PtdIns(4,5)P_2 regeneration and the continued rise of DAG and Ins(1,4,5)P_3. Our final model retained Falkenburger's rapidly developing (τ = approximately 1 s) 10-fold acceleration of both PM kinases followed by an additional slowly developing (τ = 300 s) acceleration of PM PI4K activity that gradually increased the final rate by 100-fold compared with that of the prestimulus state. We also added a Golgi PI4K activity that did not have an initial increase upon agonist addition but was also gradually accelerated up to 10-fold by a 300-s, slowly developing process.

Although the mathematical evidence for agonist-induced acceleration of kinases is strong, the underlying mechanisms are unresolved. In terms of intracellular signaling mechanisms, acceleration of lipid kinase activities occurs in two phases, one fast (a few seconds) and one slow (several minutes) during agonist action. These may involve two distinct signaling systems, or they may engage the same signal twice. Many intracellular signals are produced by M_1 receptors including DAG, Ca^{2+}, arrestin, and Ras-Raf-MEK-ERK pathways as well as depletion of several phosphoinositide pools. In the experiments of Fig. S8, we had to reject the hypothesis that the acceleration of lipid kinases needed for regeneration is a simple consequence of DAG-activated PKC. The regulation of PI 4-kinases is probably complicated. They are versatile enzymes, forming multivalent complexes with many regulatory partners (Boura and Nencka, 2015; Burke, 2018). For example, soluble PI4KIIIα is brought to the PM in a complex with EFR3 and TTC7 (Nakatsu et al., 2012) scaffolded by FAM126 (Baskin et al., 2016; Lees et al., 2017), and TTC7 is liberated from the complex by TMEM150 (Chung et al., 2015); PI4KIIIβ is stimulated by neuronal calcium sensor 1 (Nakamura et al., 2019), cholesterol (Nishimura et al., 2019), and many other partners (Burke, 2018). In addition to the EFR3B/TTC7B/PI4KIIIα complex, the literature describes EFR3B/TMEM150A/PI4KIIIα and EFR3B/CXCR4/PI4KIIIα complexes (Chung et al., 2015; Sbrissa et al., 2018). Further, the 4-kinases and 5-kinases associate with PKCμ (Nishikawa et al., 1998), and in some experiments and modeling, the 4- and 5-kinases have been postulated to act together as a complex that performs a two-step synthesis of PtdIns(4,5)P_2 directly from PtdIns (Choi et al., 2016; Olivença et al., 2018). Much more work is needed to dissect the mechanisms of the acceleration described here and to determine which subtypes of kinases are accelerated, where, and how.

Subtype(s) of PI4K and sources of PtdIns4*P*

The importance of type III PI4Ks to synthesize PM PtdIns(4,5)P_2 was recognized in decades-old studies. Measurements using ^{32}P-labeled lipids or ^{3}H-labeled inositol and 10-min applications of angiotensin II showed regeneration of PtdIns(4,5)P_2 and PtdIns4*P* as well as slowly growing Ins(1,4,5)P_3 production, all eliminated by Wtn (Nakanishi et al., 1994, 1995) and by PAO but not by PIK93 (Balla et al., 2008). Regeneration of PtdIns(4,5)P_2 and PtdIns4*P* is also blocked by the newly described selective inhibitor A1 (Bojjireddy et al., 2014). Similarly, with optical probes, Tóth et al. (2016) using angiotensin II and we in this paper using Oxo-M found that PtdIns(4,5)P_2 regeneration and growing Ins(1,4,5)P_3 production are eliminated by A1 and not by PIK93. Thus, PI4KIIIα is key for PtdIns(4,5)P_2 regeneration. Further, possible PM PtdIns4*P* regeneration was absent when we abolished PI4K activities by PAO. In fibroblasts, selective knockout of PI4KIIIα reduces total cellular PtdIns4*P* to 25% and causes some intracellular membranes to acquire PtdIns(4,5)P_2 and take up a PM-like identity (Nakatsu et al., 2012). Nakatsu et al. (2012) concluded that "targeting of PI4KIIIα to the PM is a key upstream event in defining the proteomic and lipidomic identity of [the PM]."

Where are the PI4KIIIα enzyme and the synthesis of PtdIns4*P*? It has been reported that PI4KIIIα localizes to the PM and some internal membranes and that PI4KIIIβ localizes to the Golgi (Hammond et al., 2014). The images in the Hammond et al. (2014) paper suggest to us that the most intense label for PI4KIIIα is again overlapping the Golgi region. We found overexpressed PI4KIIIα not only in the PM but also partially overlapping with TGN38 in the trans-Golgi (Fig. S5, A and B; 6 out of 10 cells), whereas we found overexpressed PI4KIIIβ in the cis-Golgi, colocalized with giantin (Fig. S5 C; 6 out of 7 cells; Luzio et al., 1990; Mardones et al., 2006). The former kinase contributes to regeneration of PtdIns(4,5)P_2, and the latter does not (Fig. 5 B; A1 versus PIK93). Bojjireddy et al. (2014) concluded that the A1-sensitive kinase is necessary for what we have called PtdIns(4,5)P_2 regeneration during PLC activation but not for PtdIns(4,5)P_2 maintenance in resting cells. This brings up the interesting concept that receptor activation may call into play a lipid kinase pathway that is different from the "housekeeping" pathway that accounts for the normal predominance of PtdIns(4,5)P_2 at the PM.

Where is the parent compound, PtdIns, the most abundant phosphoinositide? Newly developed probes reveal its significant presence in the Golgi, mitochondria, peroxisomes, and ER (Pemberton et al., 2020; Zewe et al., 2020). PtdIns is detectable but at a much lower concentration in the PM, both in resting and in receptor-stimulated cells.

Where is the PtdIns4*P* product? Significant pools of PtdIns4*P* are present in the Golgi, the small vesicles, and the PM (Hammond et al., 2014), whereas the ER harbors the transmembrane 4-phosphatase enzyme Sac1 that destroys any PtdIns4*P* there. Using the P4M probe (Hammond et al., 2014), we estimated that half of the P4M stain is in the PM and half is in the Golgi. In our modeling (Fig. 1 and Falkenburger et al., 2013) and in experimental tests (de Rubio et al., 2018), PM PtdIns4*P* is considered an alternative direct substrate of receptor-activated PLC (Table S2 and Table S4) in addition to the main substrate PtdIns(4,5)P_2. Mass spectrometry reports that 50% of the total cellular PtdIns*P* is gone after 5 s of exposure to Oxo-M (Traynor-Kaplan et al., 2017), presumably meaning that this large fraction of PtdIns*P* is immediately accessible and susceptible to rapid depletion by PLC at the PM. By 60 s, the total cellular PtdIns*P* is depleted to 25% of control.

The pool of PtdIns4*P* in the PM has puzzling properties. Although sizeable, this PM pool seems not as closely coupled to the PM PtdIns(4,5)P_2 pool as expected. Three types of experiments suggest that the PM PtdIns*P* pool is not the main precursor of PM PtdIns(4,5)P_2. (i) When the 4-phosphatase PJ-Sac1 is recruited by rapamycin dimerization to the PM, either nothing happens to the resting PM PtdIns(4,5)P_2 pool (Hammond et al., 2012; Hammond et al., 2014) or the pool is just partially but not fully depleted (Dickson et al., 2014). In either case, the remaining PtdIns(4,5)P_2 could be much further depleted by application of a receptor agonist and could still partly recover after removal of agonist. Related experiments suggest that PM PtdIns*P* can be depleted without affecting PM PtdIns(4,5)P_2 and that PM PtdIns(4,5)P_2 can be depleted without affecting PM PtdIns*P* (de Rubio et al., 2018). (ii) In our experiments, when the activity of PI4KIIIα was blocked by Wtn or A1, a small PtdIns4*P* regeneration during Oxo-M action still seemed to be occurring at the PM, suggesting that regenerating PtdIns4*P* at the PM is produced by 4-kinases other than PI4KIIIα, kinases that are not inhibited by Wtn and A1. (iii) When PJ-Sac1 is directed by rapamycin dimerization to the Golgi, the resting PM PtdIns(4,5)P_2 pool (reported by KCNQ ion channels) drops within 30 s by 40% (Dickson et al., 2014), and within just 60 s, the regeneration of PM PtdIns(4,5)P_2 (reported by $PH_{PLC\delta1}$ probes) during long agonist application is fully blocked (Fig. 6 D). Taken together, we interpret these findings to mean that during regeneration of PtdIns(4,5)P_2, much of the necessary PtdIns4*P* precursor generated by PI4KIIIα is coming from the Golgi in a protected manner that exposes it neither to dephosphorylation by the PJ-Sac1 that has been artificially translocated to the PM nor to activated PLC. Perhaps the PtdIns4*P* is converted to PtdIns(4,5)P_2 in transit (Fig. 1). To be more cautious, rather than concluding that agonist accelerates just the PI4KIIIα enzyme, we might have to say that agonist accelerates the arrows that collectively represent A1-sensitive production and/or delivery of PI4KIIIα products.

Quantitative questions that remain

Fig. 1 and our model are only approximate representations to be revised as we continue to learn more from future research. The locations of synthesis of PtdIns need better specification. Traditionally it is the ER, but are there subdomains of the ER that communicate most efficiently with the Golgi? Myo-inositol is one of the precursor ingredients for PtdIns synthesis. We have shown it can be rate limiting so that a cell that is starved for myo-inositol and unable to retrieve it from Ins(1,4,5)P_3 cannot sustain regeneration of PtdIns(4,5)P_2 beyond a few minutes (Fig. 3 E). Supplying extra myo-inositol in the medium or in the intracellular solution dramatically increased the resting PM PtdIns(4,5)P_2 pools in 2 h or 12 min, respectively (Dai et al.,

2016). Unexpectedly, however, mass spectrometry revealed that exposing cells to myo-inositol overnight did not increase the total cellular amount (in all pools) of the necessary parent compound PtdIns (Dai et al., 2016), although it almost doubled the total amount of cellular PtdInsP_2 and PtdIns$P$. Perhaps of the many recently identified pools of PtdIns listed above, only a small subset is effectively in the pipeline to generate PtdIns4P and PM PtdIns(4,5)P_2 during receptor activation. Possibly, the Golgi and the ER or just subdomains of these organelles, such as the trans-Golgi, supply the precursor for PtdIns4P and PtdIns(4,5)P_2 synthesis. In this way, the other larger pools of PtdIns are off the express track and are not affected. The dynamics of the pools of PtdIns and of the precursors myo-inositol and phosphatidic acid remain to be determined.

There are other issues. How would Golgi PtdIns4P be delivered to the PM? What are the molecular determinants of the unconventional reaction arrow between the Golgi and the PM lumping a lipid transfer with a 5-kinase (Fig. 1), and how else does Golgi PtdIns4P get to the PM? What are the kinetic parameters and pools of lipid exchange reactions, such as the coupled PtdIns/phosphatidic acid exchange reaction represented as separate arrows on the far left and far right of the figure (inspired by Nir2; Chang and Liou, 2015; Kim et al., 2015) or retrograde transfer of PtdIns4P to the ER by oxysterol-binding protein–related proteins (ORPs; Sohn et al., 2018)? Does Golgi PtdIns4P hydrolysis by activation of PLCβ directly affect PtdIns(4,5)P_2 regeneration? Does a pool of PtdIns5P contribute significantly to PtdIns(4,5)P_2 regeneration? Can these processes be incorporated into a self-consistent model?

Conclusions

Activation of muscarinic receptors engages both an early fast and a second gradual but large acceleration of lipid kinases. An accelerated PI4KIIIα pathway participates in the regeneration of PM PtdIns(4,5)P_2 but is less important for regeneration of PM PtdIns4P. Regeneration of PM PtdIns(4,5)P_2 depends on PtdIns4P synthesized elsewhere, including in the Golgi.

Acknowledgments

Jeanne M. Nerbonne served as editor.

We thank Lea M. Miller for technical assistance, Dr. Alexis Traynor-Kaplan for help with mass spectrometry, and Drs. Bjoern Falkenburger, Jill B. Jensen, Martin Kruse, Luis Vaca, and Oscar Vivas for insightful comments on the manuscript.

This work was supported by a grant from the National Institutes of Health (R37-NS08174), by the Basic Science Research Program through the National Research Foundation of Korea funded by the Ministry of Education (2019R1A6A3A03031486), and by the Wayne E. Crill Endowed Professorship. The Virtual Cell is supported by the National Institute of General Medical Sciences/National Institutes of Health (grant R24 GM137787).

The authors declare no competing financial interests.

Author contributions: J. Myeong, L. de la Cruz, S.-R. Jung, J.-H. Yeon, B.-C. Suh, D.-S. Koh, and B. Hille designed and planned the experiments. J. Myeong, L. de la Cruz, J.-H. Yeon, and S.R. Jung performed the experiments. J. Myeong analyzed the data. J. Myeong, D.-S. Koh, and B. Hille interpreted the data and wrote the paper.

Submitted: 11 April 2020
Accepted: 13 October 2020

References

Anderson, K.E., A. Kielkowska, T.N. Durrant, V. Juvin, J. Clark, L.R. Stephens, and P.T. Hawkins. 2013. Lysophosphatidylinositol-acyltransferase-1 (LPIAT1) is required to maintain physiological levels of PtdIns and PtdInsP_2 in the mouse. *PLoS One.* 8. e58425. https://doi.org/10.1371/journal.pone.0058425

Balla, T. 2013. Phosphoinositides: tiny lipids with giant impact on cell regulation. *Physiol. Rev.* 93:1019–1137. https://doi.org/10.1152/physrev.00028.2012

Balla, A., G. Tuymetova, A. Tsiomenko, P. Várnai, and T. Balla. 2005. A plasma membrane pool of phosphatidylinositol 4-phosphate is generated by phosphatidylinositol 4-kinase type-III alpha: studies with the PH domains of the oxysterol binding protein and FAPP1. *Mol. Biol. Cell.* 16:1282–1295. https://doi.org/10.1091/mbc.e04-07-0578

Balla, A., Y.J. Kim, P. Varnai, Z. Szentpetery, Z. Knight, K.M. Shokat, and T. Balla. 2008. Maintenance of hormone-sensitive phosphoinositide pools in the plasma membrane requires phosphatidylinositol 4-kinase IIIalpha. *Mol. Biol. Cell.* 19:711–721. https://doi.org/10.1091/mbc.e07-07-0713

Baskin, J.M., X. Wu, R. Christiano, M.S. Oh, C.M. Schauder, E. Gazzerro, M. Messa, S. Baldassari, S. Assereto, R. Biancheri, et al. 2016. The leukodystrophy protein FAM126A (hyccin) regulates PtdIns(4)P synthesis at the plasma membrane. *Nat. Cell Biol.* 18:132–138. https://doi.org/10.1038/ncb3271

Berridge, M.J., C.P. Downes, and M.R. Hanley. 1989. Neural and developmental actions of lithium: a unifying hypothesis. *Cell.* 59:411–419. https://doi.org/10.1016/0092-8674(89)90026-3

Bojjireddy, N., J. Botyanszki, G. Hammond, D. Creech, R. Peterson, D.C. Kemp, M. Snead, R. Brown, A. Morrison, S. Wilson, et al. 2014. Pharmacological and genetic targeting of the PI4KA enzyme reveals its important role in maintaining plasma membrane phosphatidylinositol 4-phosphate and phosphatidylinositol 4,5-bisphosphate levels. *J. Biol. Chem.* 289:6120–6132. https://doi.org/10.1074/jbc.M113.531426

Bojjireddy, N., M.L. Guzman-Hernandez, N.R. Reinhard, M. Jovic, and T. Balla. 2015. EFR3s are palmitoylated plasma membrane proteins that control responsiveness to G-protein-coupled receptors. *J. Cell Sci.* 128:118–128. https://doi.org/10.1242/jcs.157495

Boura, E., and R. Nencka. 2015. Phosphatidylinositol 4-kinases: Function, structure, and inhibition. *Exp. Cell Res.* 337:136–145. https://doi.org/10.1016/j.yexcr.2015.03.028

Burke, J.E. 2018. Structural Basis for Regulation of Phosphoinositide Kinases and Their Involvement in Human Disease. *Mol. Cell.* 71:653–673. https://doi.org/10.1016/j.molcel.2018.08.005

Chang, C.L., and J. Liou. 2015. Phosphatidylinositol 4,5-Bisphosphate Homeostasis Regulated by Nir2 and Nir3 Proteins at Endoplasmic Reticulum-Plasma Membrane Junctions. *J. Biol. Chem.* 290:14289–14301. https://doi.org/10.1074/jbc.M114.621375

Choi, J., J. Chen, S.L. Schreiber, and J. Clardy. 1996. Structure of the FKBP12-rapamycin complex interacting with the binding domain of human FRAP. *Science.* 273:239–242. https://doi.org/10.1126/science.273.5272.239

Choi, S., A.C. Hedman, S. Sayedyahossein, N. Thapa, D.B. Sacks, and R.A. Anderson. 2016. Agonist-stimulated phosphatidylinositol-3,4,5-trisphosphate generation by scaffolded phosphoinositide kinases. *Nat. Cell Biol.* 18:1324–1335. https://doi.org/10.1038/ncb3441

Chung, J., F. Nakatsu, J.M. Baskin, and P. De Camilli. 2015. Plasticity of PI4KIIIα interactions at the plasma membrane. *EMBO Rep.* 16:312–320. https://doi.org/10.15252/embr.201439151

Cowan, A.E., I.I. Moraru, J.C. Schaff, B.M. Slepchenko, and L.M. Loew. 2012. Spatial modeling of cell signaling networks. *Methods Cell Biol.* 110:195–221. https://doi.org/10.1016/B978-0-12-388403-9.00008-4

Dai, G., H. Yu, M. Kruse, A. Traynor-Kaplan, and B. Hille. 2016. Osmoregulatory inositol transporter SMIT1 modulates electrical activity by adjusting PI(4,5)P_2 levels. *Proc. Natl. Acad. Sci. USA.* 113:E3290–E3299. https://doi.org/10.1073/pnas.1606348113

de Barry, J., A. Janoshazi, J.L. Dupont, O. Procksch, S. Chasserot-Golaz, A. Jeromin, and N. Vitale. 2006. Functional implication of neuronal calcium sensor-1 and phosphoinositol 4-kinase-β interaction in regulated

exocytosis of PC12 cells. *J. Biol. Chem.* 281:18098–18111. https://doi.org/10.1074/jbc.M509842200

de Rubio, R.G., R.F. Ransom, S. Malik, D.I. Yule, A. Anantharam, and A.V. Smrcka. 2018. Phosphatidylinositol 4-phosphate is a major source of GPCR-stimulated phosphoinositide production. *Sci. Signal.* 11:eaan1210. https://doi.org/10.1126/scisignal.aan1210

Dickson, E.J., and B. Hille. 2019. Understanding phosphoinositides: rare, dynamic, and essential membrane phospholipids. *Biochem. J.* 476:1–23. https://doi.org/10.1042/BCJ20180022

Dickson, E.J., B.H. Falkenburger, and B. Hille. 2013. Quantitative properties and receptor reserve of the IP_3 and calcium branch of G_q-coupled receptor signaling. *J. Gen. Physiol.* 141:521–535. https://doi.org/10.1085/jgp.201210886

Dickson, E.J., J.B. Jensen, and B. Hille. 2014. Golgi and plasma membrane pools of PI(4)P contribute to plasma membrane $PI(4,5)P_2$ and maintenance of KCNQ2/3 ion channel current. *Proc. Natl. Acad. Sci. USA.* 111: E2281–E2290. https://doi.org/10.1073/pnas.1407133111

Erickson, M.G., B.A. Alseikhan, B.Z. Peterson, and D.T. Yue. 2001. Preassociation of calmodulin with voltage-gated Ca^{2+} channels revealed by FRET in single living cells. *Neuron.* 31:973–985. https://doi.org/10.1016/S0896-6273(01)00438-X

Falkenburger, B.H., J.B. Jensen, and B. Hille. 2010. Kinetics of PIP_2 metabolism and KCNQ2/3 channel regulation studied with a voltage-sensitive phosphatase in living cells. *J. Gen. Physiol.* 135:99–114. https://doi.org/10.1085/jgp.200910345

Falkenburger, B.H., E.J. Dickson, and B. Hille. 2013. Quantitative properties and receptor reserve of the DAG and PKC branch of G_q-coupled receptor signaling. *J. Gen. Physiol.* 141:537–555. https://doi.org/10.1085/jgp.201210887

Hallcher, L.M., and W.R. Sherman. 1980. The effects of lithium ion and other agents on the activity of myo-inositol-1-phosphatase from bovine brain. *J. Biol. Chem.* 255:10896–10901.

Hammond, G.R., M.J. Fischer, K.E. Anderson, J. Holdich, A. Koteci, T. Balla, and R.F. Irvine. 2012. PI4P and $PI(4,5)P_2$ are essential but independent lipid determinants of membrane identity. *Science.* 337:727–730. https://doi.org/10.1126/science.1222483

Hammond, G.R., M.P. Machner, and T. Balla. 2014. A novel probe for phosphatidylinositol 4-phosphate reveals multiple pools beyond the Golgi. *J. Cell Biol.* 205:113–126. https://doi.org/10.1083/jcb.201312072

Hansen, S.H., A. Olsson, and J.E. Casanova. 1995. Wortmannin, an inhibitor of phosphoinositide 3-kinase, inhibits transcytosis in polarized epithelial cells. *J. Biol. Chem.* 270:28425–28432. https://doi.org/10.1074/jbc.270.47.28425

Hille, B., E.J. Dickson, M. Kruse, O. Vivas, and B.C. Suh. 2015. Phosphoinositides regulate ion channels. *Biochim. Biophys. Acta.* 1851:844–856. https://doi.org/10.1016/j.bbalip.2014.09.010

Hirose, K., S. Kadowaki, M. Tanabe, H. Takeshima, and M. Iino. 1999. Spatiotemporal dynamics of inositol 1,4,5-trisphosphate that underlies complex Ca^{2+} mobilization patterns. *Science.* 284:1527–1530. https://doi.org/10.1126/science.284.5419.1527

Horowitz, L.F., W. Hirdes, B.C. Suh, D.W. Hilgemann, K. Mackie, and B. Hille. 2005. Phospholipase C in living cells: activation, inhibition, Ca^{2+} requirement, and regulation of M current. *J. Gen. Physiol.* 126:243–262. https://doi.org/10.1085/jgp.200509309

Inoue, T., W.D. Heo, J.S. Grimley, T.J. Wandless, and T. Meyer. 2005. An inducible translocation strategy to rapidly activate and inhibit small GTPase signaling pathways. *Nat. Methods.* 2:415–418. https://doi.org/10.1038/nmeth763

Itsuki, K., Y. Imai, H. Hase, Y. Okamura, R. Inoue, and M.X. Mori. 2014. PLC-mediated $PI(4,5)P_2$ hydrolysis regulates activation and inactivation of TRPC6/7 channels. *J. Gen. Physiol.* 143:183–201. https://doi.org/10.1085/jgp.201311033

Jung, S.R., J.B. Seo, Y. Deng, C.L. Asbury, B. Hille, and D.S. Koh. 2016. Contributions of protein kinases and β-arrestin to termination of protease-activated receptor 2 signaling. *J. Gen. Physiol.* 147:255–271. https://doi.org/10.1085/jgp.201511477

Jung, S.R., C. Kushmerick, J.B. Seo, D.S. Koh, and B. Hille. 2017. Muscarinic receptor regulates extracellular signal regulated kinase by two modes of arrestin binding. *Proc. Natl. Acad. Sci. USA.* 114:E5579–E5588. https://doi.org/10.1073/pnas.1700331114

Keum, D., M. Kruse, D.I. Kim, B. Hille, and B.C. Suh. 2016. Phosphoinositide 5- and 3-phosphatase activities of a voltage-sensing phosphatase in living cells show identical voltage dependence. *Proc. Natl. Acad. Sci. USA.* 113: E3686–E3695. https://doi.org/10.1073/pnas.1606472113

Kienitz, M.C., D. Vladimirova, C. Müller, L. Pott, and A. Rinne. 2016. Receptor Species-dependent Desensitization Controls KCNQ1/KCNE1 K^+ Channels as Downstream Effectors of G_q Protein-coupled Receptors. *J. Biol. Chem.* 291:26410–26426. https://doi.org/10.1074/jbc.M116.746974

Kim, Y.J., M.L. Guzman-Hernandez, E. Wisniewski, and T. Balla. 2015. Phosphatidylinositol-Phosphatidic Acid Exchange by Nir2 at ER-PM Contact Sites Maintains Phosphoinositide Signaling Competence. *Dev. Cell.* 33:549–561. https://doi.org/10.1016/j.devcel.2015.04.028

Kirk, C.J., J.A. Creba, C.P. Downes, and R.H. Michell. 1981. Hormone-stimulated metabolism of inositol lipids and its relationship to hepatic receptor function. *Biochem. Soc. Trans.* 9:377–379. https://doi.org/10.1042/bst0090377

Ko, J., J. Myeong, M. Kwak, J.H. Jeon, and I. So. 2019a. Identification of phospholipase C β downstream effect on transient receptor potential canonical 1/4, transient receptor potential canonical 1/5 channels. *Korean J. Physiol. Pharmacol.* 23:357–366. https://doi.org/10.4196/kjpp.2019.23.5.357

Ko, J., J. Myeong, Y.C. Shin, and I. So. 2019b. Differential $PI(4,5)P_2$ sensitivities of TRPC4, C5 homomeric and TRPC1/4, C1/5 heteromeric channels. *Sci. Rep.* 9:1849. https://doi.org/10.1038/s41598-018-38443-0

Komatsu, T., I. Kukelyansky, J.M. McCaffery, T. Ueno, L.C. Varela, and T. Inoue. 2010. Organelle-specific, rapid induction of molecular activities and membrane tethering. *Nat. Methods.* 7:206–208. https://doi.org/10.1038/nmeth.1428

Lees, J.A., Y. Zhang, M.S. Oh, C.M. Schauder, X. Yu, J.M. Baskin, K. Dobbs, L.D. Notarangelo, P. De Camilli, T. Walz, and K.M. Reinisch. 2017. Architecture of the human PI4KIIIα lipid kinase complex. *Proc. Natl. Acad. Sci. USA.* 114:13720–13725. https://doi.org/10.1073/pnas.1718471115

Li, Y., N. Gamper, D.W. Hilgemann, and M.S. Shapiro. 2005. Regulation of Kv7 (KCNQ) K^+ channel open probability by phosphatidylinositol 4,5-bisphosphate. *J. Neurosci.* 25:9825–9835. https://doi.org/10.1523/JNEUROSCI.2597-05.2005

Liang, H., S. He, J. Yang, X. Jia, P. Wang, X. Chen, Z. Zhang, X. Zou, M.A. McNutt, W.H. Shen, and Y. Yin. 2014. PTENα, a PTEN isoform translated through alternative initiation, regulates mitochondrial function and energy metabolism. *Cell Metab.* 19:836–848. https://doi.org/10.1016/j.cmet.2014.03.023

Liu, Y., R.A. Kahn, and J.H. Prestegard. 2014. Interaction of Fapp1 with Arf1 and PI4P at a membrane surface: an example of coincidence detection. *Structure.* 22:421–430. https://doi.org/10.1016/j.str.2013.12.011

Luzio, J.P., B. Brake, G. Banting, K.E. Howell, P. Braghetta, and K.K. Stanley. 1990. Identification, sequencing and expression of an integral membrane protein of the trans-Golgi network (TGN38). *Biochem. J.* 270: 97–102. https://doi.org/10.1042/bj2700097

Mardones, G.A., C.M. Snyder, and K.E. Howell. 2006. *Cis*-Golgi matrix proteins move directly to endoplasmic reticulum exit sites by association with tubules. *Mol. Biol. Cell.* 17:525–538. https://doi.org/10.1091/mbc.e05-05-0447

Myeong, J., M. Kwak, J.P. Jeon, C. Hong, J.H. Jeon, and I. So. 2015. Close spatio-association of the transient receptor potential canonical 4 (TRPC4) channel with $G\alpha_i$ in TRPC4 activation process. *Am. J. Physiol. Cell Physiol.* 308:C879–C889. https://doi.org/10.1152/ajpcell.00374.2014

Myeong, J., J. Ko, M. Kwak, J. Kim, J. Woo, K. Ha, C. Hong, D. Yang, H.J. Kim, J.H. Jeon, and I. So. 2018. Dual action of the $G\alpha_q$-PLCβ-$PI(4,5)P_2$ pathway on TRPC1/4 and TRPC1/5 heterotetramers. *Sci. Rep.* 8:12117. https://doi.org/10.1038/s41598-018-30625-0

Nakamura, T.Y., S. Nakao, and S. Wakabayashi. 2019. Emerging Roles of Neuronal Ca^{2+} Sensor-1 in Cardiac and Neuronal Tissues: A Mini Review. *Front. Mol. Neurosci.* 12:56. https://doi.org/10.3389/fnmol.2019.00056

Nakanishi, S., K.J. Catt, and T. Balla. 1994. Inhibition of agonist-stimulated inositol 1,4,5-trisphosphate production and calcium signaling by the myosin light chain kinase inhibitor, wortmannin. *J. Biol. Chem.* 269: 6528–6535.

Nakanishi, S., K.J. Catt, and T. Balla. 1995. A wortmannin-sensitive phosphatidylinositol 4-kinase that regulates hormone-sensitive pools of inositolphospholipids. *Proc. Natl. Acad. Sci. USA.* 92:5317–5321. https://doi.org/10.1073/pnas.92.12.5317

Nakatsu, F., J.M. Baskin, J. Chung, L.B. Tanner, G. Shui, S.Y. Lee, M. Pirruccello, M. Hao, N.T. Ingolia, M.R. Wenk, and P. De Camilli. 2012. PtdIns4P synthesis by PI4KIIIα at the plasma membrane and its impact on plasma membrane identity. *J. Cell Biol.* 199:1003–1016. https://doi.org/10.1083/jcb.201206095

Nishikawa, K., A. Toker, K. Wong, P.A. Marignani, F.J. Johannes, and L.C. Cantley. 1998. Association of protein kinase Cmu with type II

phosphatidylinositol 4-kinase and type I phosphatidylinositol-4-phosphate 5-kinase. *J. Biol. Chem.* 273:23126–23133. https://doi.org/10.1074/jbc.273.36.23126

Nishimura, T., M. Gecht, R. Covino, G. Hummer, M.A. Surma, C. Klose, H. Arai, N. Kono, and C.J. Stefan. 2019. Osh Proteins Control Nanoscale Lipid Organization Necessary for PI(4,5)P_2 Synthesis. *Mol. Cell.* 75: 1043–1057.e8. https://doi.org/10.1016/j.molcel.2019.06.037

Olivença, D.V., I. Uliyakina, L.L. Fonseca, M.D. Amaral, E.O. Voit, and F.R. Pinto. 2018. A Mathematical Model of the Phosphoinositide Pathway. *Sci. Rep.* 8:3904. https://doi.org/10.1038/s41598-018-22226-8

Pemberton, J.G., Y.J. Kim, J. Humpolickova, A. Eisenreichova, N. Sengupta, D.J. Toth, E. Boura, and T. Balla. 2020. Defining the subcellular distribution and metabolic channeling of phosphatidylinositol. *J. Cell Biol.* 219: e201906130. https://doi.org/10.1083/jcb.201906130

Quinn, K.V., P. Behe, and A. Tinker. 2008. Monitoring changes in membrane phosphatidylinositol 4,5-bisphosphate in living cells using a domain from the transcription factor tubby. *J. Physiol.* 586:2855–2871. https://doi.org/10.1113/jphysiol.2008.153791

Sbrissa, D., G. Naisan, O.C. Ikonomov, and A. Shisheva. 2018. Apilimod, a candidate anticancer therapeutic, arrests not only PtdIns(3,5)P_2 but also PtdIns5P synthesis by PIKfyve and induces bafilomycin A1-reversible aberrant endomembrane dilation. *PLoS One.* 13:e0204532. https://doi.org/10.1371/journal.pone.0204532

Schaff, J., C.C. Fink, B. Slepchenko, J.H. Carson, and L.M. Loew. 1997. A general computational framework for modeling cellular structure and function. *Biophys. J.* 73:1135–1146. https://doi.org/10.1016/S0006-3495(97)78146-3

Sherman, W.R., L.Y. Munsell, B.G. Gish, and M.P. Honchar. 1985. Effects of systemically administered lithium on phosphoinositide metabolism in rat brain, kidney, and testis. *J. Neurochem.* 44:798–807. https://doi.org/10.1111/j.1471-4159.1985.tb12886.x

Sims, C.E., and N.L. Allbritton. 1998. Metabolism of inositol 1,4,5-trisphosphate and inositol 1,3,4,5-tetrakisphosphate by the oocytes of Xenopus laevis. *J. Biol. Chem.* 273:4052–4058. https://doi.org/10.1074/jbc.273.7.4052

Sohn, M., M. Korzeniowski, J.P. Zewe, R.C. Wills, G.R.V. Hammond, J. Humpolickova, L. Vrzal, D. Chalupska, V. Veverka, G.D. Fairn, et al. 2018. PI(4,5)P_2 controls plasma membrane PI4P and PS levels via ORP5/8 recruitment to ER-PM contact sites. *J. Cell Biol.* 217:1797–1813. https://doi.org/10.1083/jcb.201710095

Suh, B.C., and B. Hille. 2006. Does diacylglycerol regulate KCNQ channels? *Pflugers Arch.* 453:293–301. https://doi.org/10.1007/s00424-006-0092-3

Szentpetery, Z., A. Balla, Y.J. Kim, M.A. Lemmon, and T. Balla. 2009. Live cell imaging with protein domains capable of recognizing phosphatidylinositol 4,5-bisphosphate; a comparative study. *BMC Cell Biol.* 10:67. https://doi.org/10.1186/1471-2121-10-67

Szentpetery, Z., P. Várnai, and T. Balla. 2010. Acute manipulation of Golgi phosphoinositides to assess their importance in cellular trafficking and signaling. *Proc. Natl. Acad. Sci. USA.* 107:8225–8230. https://doi.org/10.1073/pnas.1000157107

Tanimura, A., A. Nezu, T. Morita, R.J. Turner, and Y. Tojyo. 2004. Fluorescent biosensor for quantitative real-time measurements of inositol 1,4,5-trisphosphate in single living cells. *J. Biol. Chem.* 279:38095–38098. https://doi.org/10.1074/jbc.C400312200

Tóth, J.T., G. Gulyás, D.J. Tóth, A. Balla, G.R. Hammond, L. Hunyady, T. Balla, and P. Várnai. 2016. BRET-monitoring of the dynamic changes of inositol lipid pools in living cells reveals a PKC-dependent PtdIns4*P* increase upon EGF and M3 receptor activation. *Biochim. Biophys. Acta.* 1861:177–187. https://doi.org/10.1016/j.bbalip.2015.12.005

Traynor-Kaplan, A., M. Kruse, E.J. Dickson, G. Dai, O. Vivas, H. Yu, D. Whittington, and B. Hille. 2017. Fatty-acyl chain profiles of cellular phosphoinositides. *Biochim. Biophys. Acta Mol. Cell Biol. Lipids.* 1862: 513–522. https://doi.org/10.1016/j.bbalip.2017.02.002

van Rheenen, J., E.M. Achame, H. Janssen, J. Calafat, and K. Jalink. 2005. PIP_2 signaling in lipid domains: a critical re-evaluation. *EMBO J.* 24: 1664–1673. https://doi.org/10.1038/sj.emboj.7600655

Willars, G.B., S.R. Nahorski, and R.A. Challiss. 1998. Differential regulation of muscarinic acetylcholine receptor-sensitive polyphosphoinositide pools and consequences for signaling in human neuroblastoma cells. *J. Biol. Chem.* 273:5037–5046. https://doi.org/10.1074/jbc.273.9.5037

Xu, C., J. Watras, and L.M. Loew. 2003. Kinetic analysis of receptor-activated phosphoinositide turnover. *J. Cell Biol.* 161:779–791. https://doi.org/10.1083/jcb.200301070

Zaika, O., L.S. Lara, N. Gamper, D.W. Hilgemann, D.B. Jaffe, and M.S. Shapiro. 2006. Angiotensin II regulates neuronal excitability via phosphatidylinositol 4,5-bisphosphate-dependent modulation of Kv7 (M-type) K^+ channels. *J. Physiol.* 575:49–67. https://doi.org/10.1113/jphysiol.2006.114074

Zaika, O., G.P. Tolstykh, D.B. Jaffe, and M.S. Shapiro. 2007. Inositol triphosphate-mediated Ca^{2+} signals direct purinergic P2Y receptor regulation of neuronal ion channels. *J. Neurosci.* 27:8914–8926. https://doi.org/10.1523/JNEUROSCI.1739-07.2007

Zewe, J.P., A.M. Miller, S. Sangappa, R.C. Wills, B.D. Goulden, and G.R.V. Hammond. 2020. Probing the subcellular distribution of phosphatidylinositol reveals a surprising lack at the plasma membrane. *J. Cell Biol.* 219:e201906127. https://doi.org/10.1083/jcb.201906127

Supplemental material

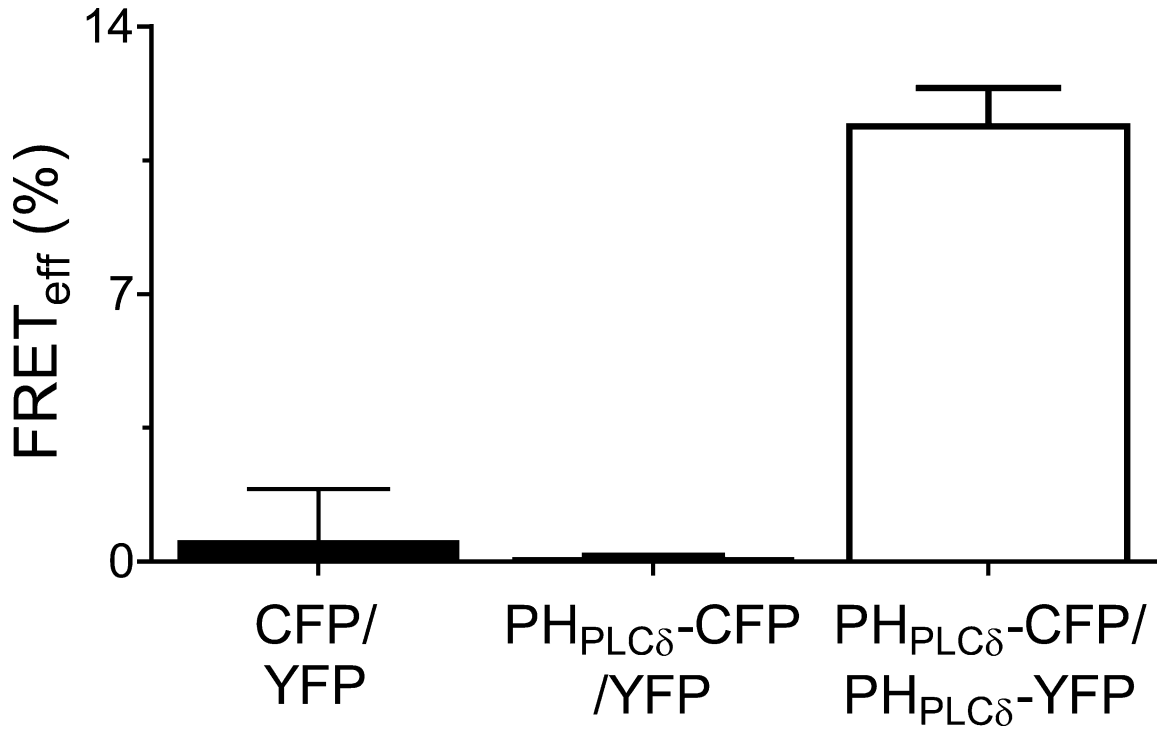

Figure S1. **Validation of three-cube FRET.** Low resting $FRET_{eff}$ between intracellular soluble CFP and soluble YFP (n = 7 cells) or between $PH_{PLC\delta1}$-CFP and soluble YFP (n = 30 cells). High homologous $FRET_{eff}$ between $PH_{PLC\delta1}$-CFP and $PH_{PLC\delta1}$-YFP probes (n = 39) in resting cells with a high concentration of PM PtdIns(4,5)P_2.

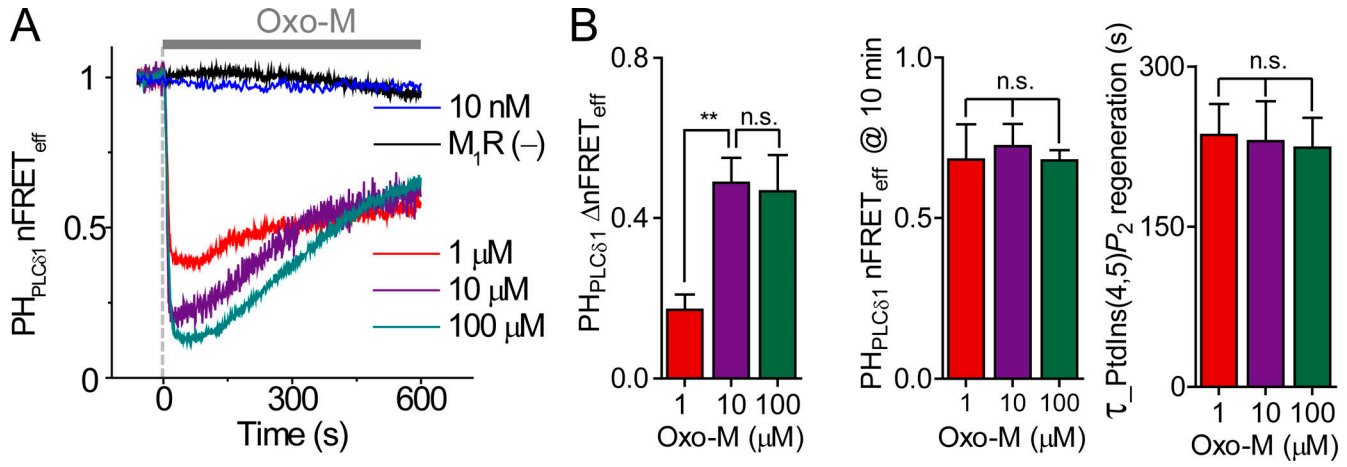

Figure S2. **PtdIns(4,5)P_2 regeneration followed initial depletion by receptor stimulation. (A)** Time course of PtdIns(4,5)P_2 indicator homologous $nFRET_{eff}$ during treatment (gray bar) with different Oxo-M concentrations in cells overexpressing M_1R. The black line is for a control cell without M_1R overexpression (M_1R (–)). **(B)** Mean of $\Delta nFRET_{eff}$, final $nFRET_{eff}$ after 10 min in Oxo-M, and the time constant of $nFRET_{eff}$ regeneration during Oxo-M application. 1 μM, n = 7 cells; 10 μM, n = 8; and 100 μM, n = 6. **, P < 0.005. n.s. not significant.

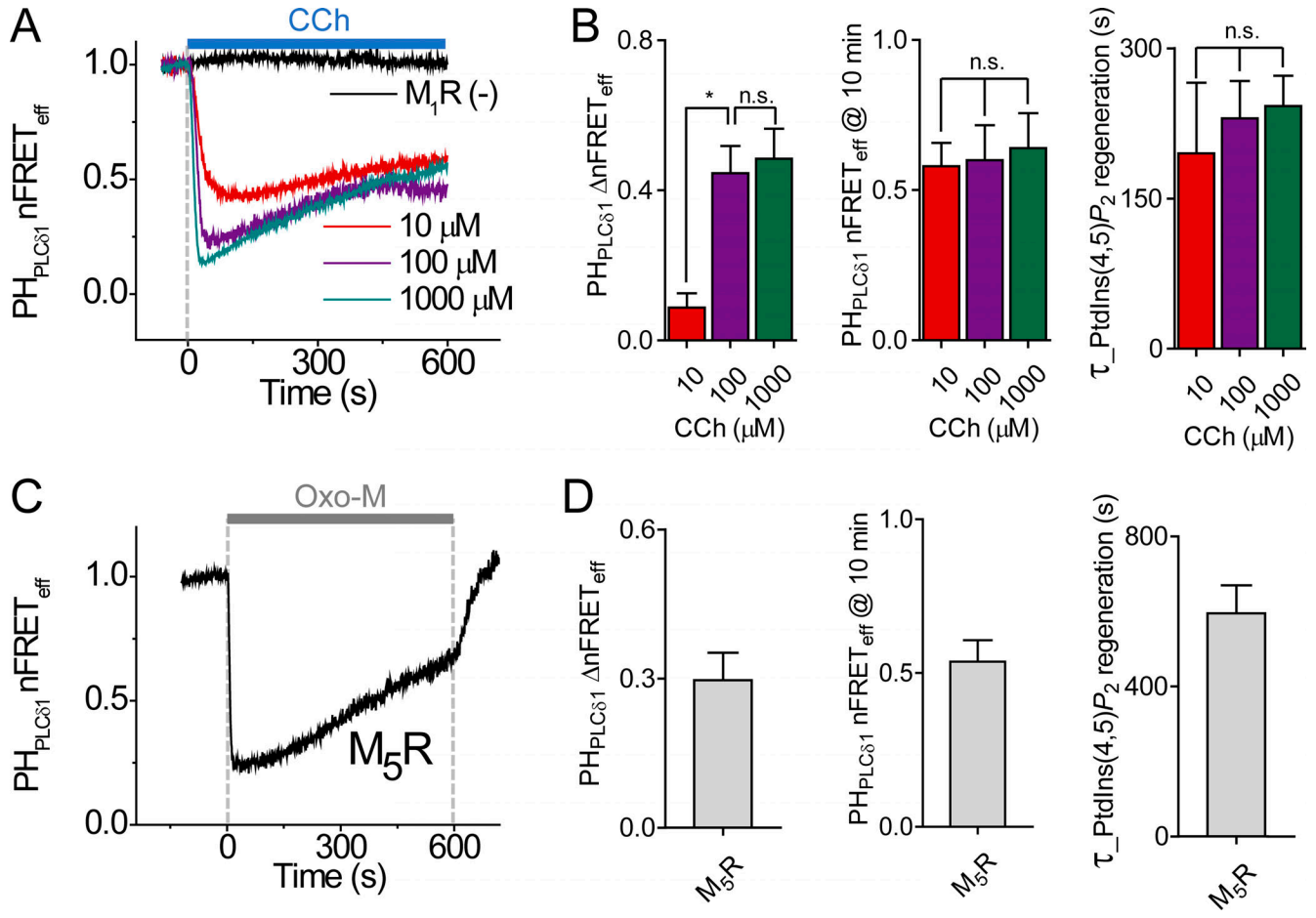

Figure S3. **Comparison of PtdIns(4,5)P_2 regeneration during stimulation with different muscarinic agonists and receptors. (A)** Time course of homologous $nFRET_{eff}$ between CFP- and YFP-tagged $PH_{PLC\delta1}$ domains during application of carbachol (light blue bar, CCh) for 10 min. Cells were transfected with the probes with or without (–) M_1R. **(B)** Mean of $\Delta nFRET_{eff}$, $nFRET_{eff}$ after 10-min CCh stimulation, and the time constant of $nFRET_{eff}$ regeneration. 10 μM, n = 4 cells; 100 μM, n = 12; and 1,000 μM, n = 5. **(C)** Time course of $nFRET_{eff}$ during application of 10 μM Oxo-M (gray bar) to cells expressing M_5R. **(D)** Summary of $\Delta nFRET_{eff}$, $nFRET_{eff}$ at 10 min, and the time constant of $nFRET_{eff}$ regeneration for cells expressing M_5R. n = 5 cells. *, P < 0.05. n.s. not significant.

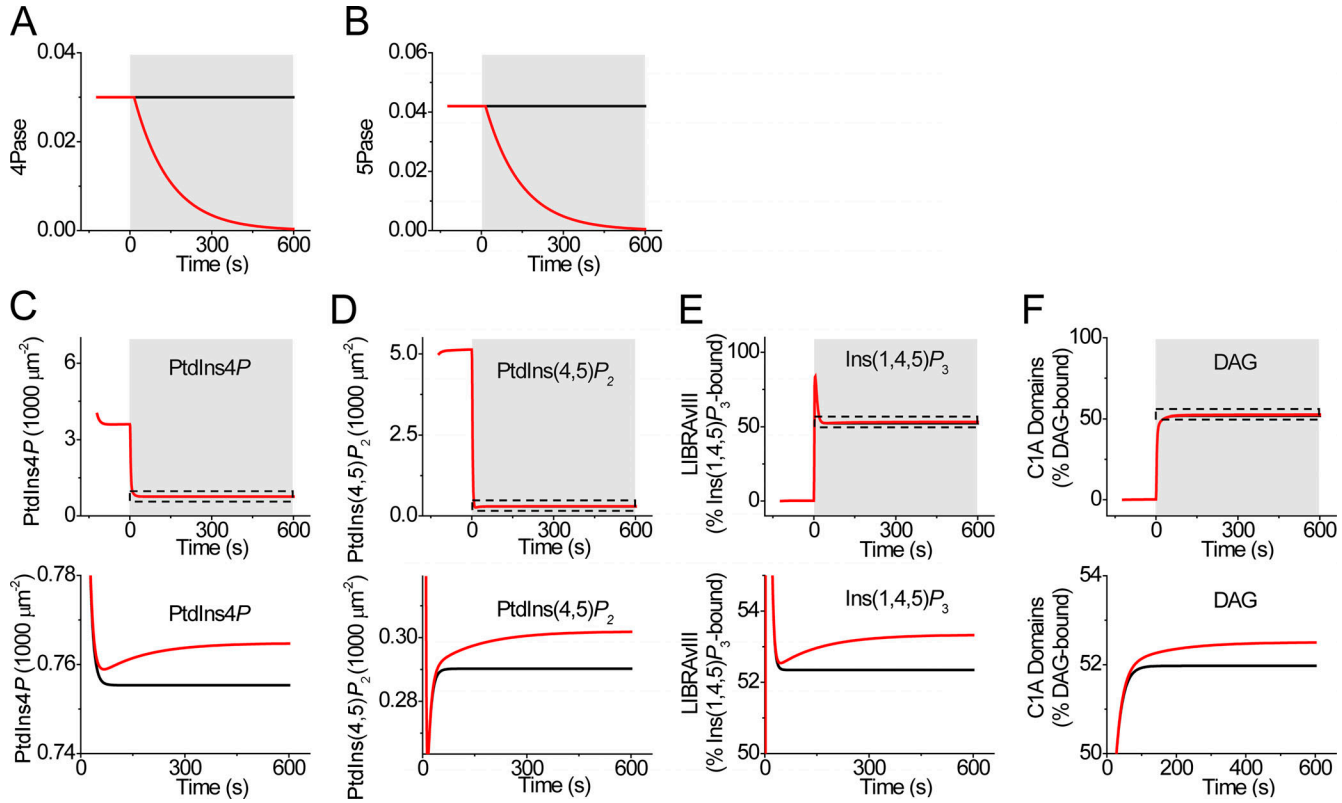

Figure S4. **Mathematical model assuming inhibition of phosphatase activities during receptor activation. (A and B)** Assumed deceleration of 4-phosphatase (4-Pase; A) and 5-phosphatase (5-Pase; B) during receptor activation (shaded area). **(C–F)** Simulated time course of PM PtdIns4*P* (C), PM PtdIns(4,5)P_2 (D), Ins(1,4,5)P_3 interacting with LIBRAvIII (E), and DAG interacting with C1A domains (F). Magnified traces underneath are expanded to reveal the tiny effects of phosphatase inhibition.

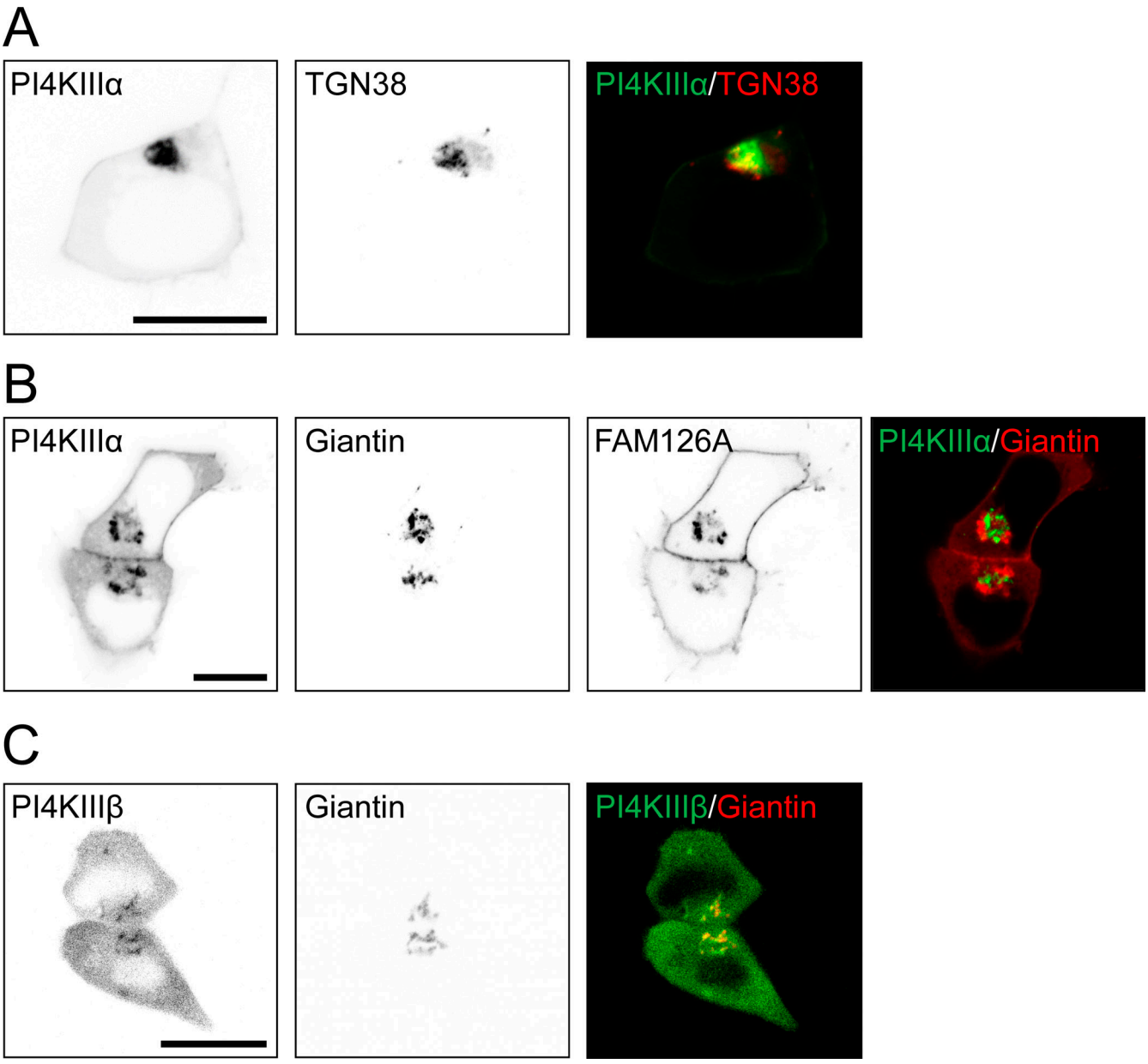

Figure S5. **Intracellular distribution of PI4KIIIα and PI4KIIIβ. (A and B)** Confocal images of GFP-tagged PI4KIIIα compared with CFP-tagged TGN38 or giantin as trans-Golgi and cis-Golgi markers, respectively. The cells coexpressed TTC7 and EFR3 with (B) or without (A) FAM126A. **(C)** Confocal images of GFP-tagged PI4KIIIβ and CFP-tagged giantin. Black-and-white images show fluorescence in reversed contrast (black). Color images overlay PI4K (green) and a Golgi marker (red). Scale bar, 10 µm.

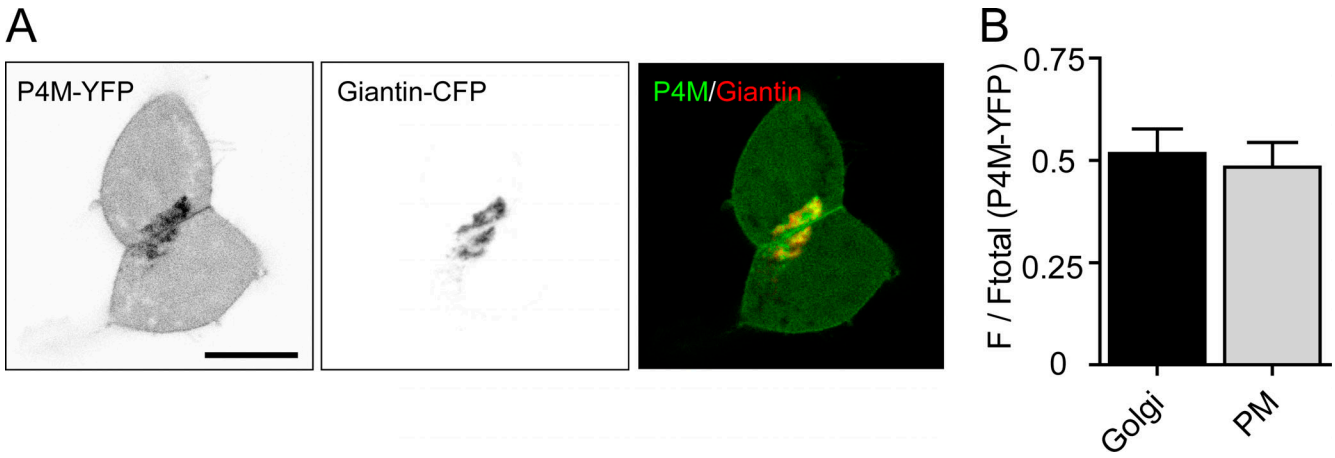

Figure S6. **Localization of PtdIns4*P* at the Golgi and PM. (A)** Left and center: Confocal images of YFP-tagged P4M and CFP-tagged giantin serving as PtdIns4P and Golgi indicators, respectively. Right: Overlay of P4M (green) and giantin (red). Scale bar, 10 µm. **(B)** Fractional partitioning of P4M-YFP fluorescence between the Golgi and PM. z-Stacks of confocal images were integrated to estimate relative P4M near the Golgi and near the PM (see Materials and methods). *n* = 9 cells. F/Ftotal, integrated fluorescence in the Golgi or PM divided by the total fluorescence in the cell.

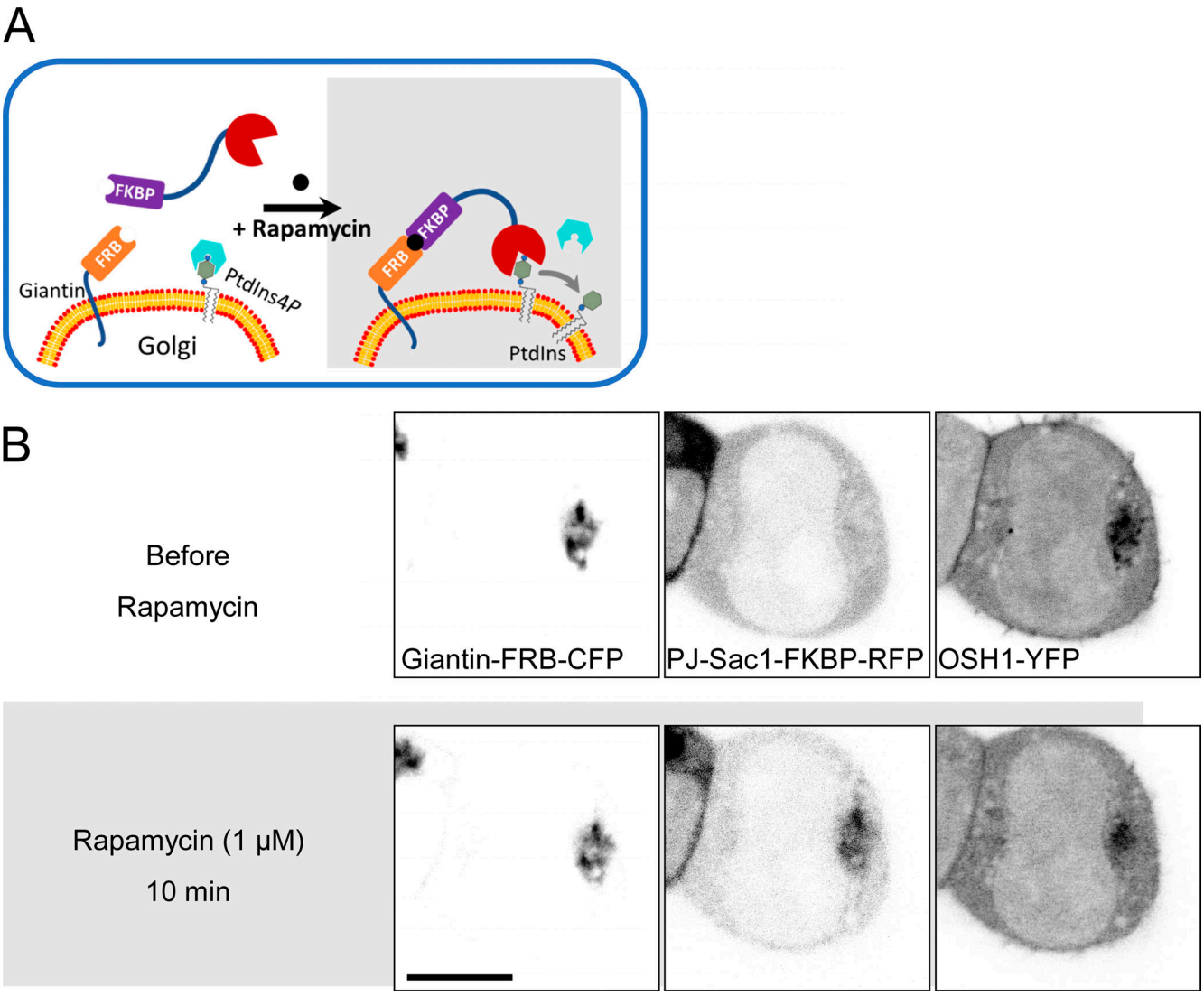

Figure S7. **Rapamycin-inducible PJ-Sac1 recruitment to the Golgi. (A)** Schematic of a cell expressing soluble PJ-Sac1 and Golgi-anchored giantin-FRB. Rapamycin, by cross-linking FKBP and FRB, recruits PJ-Sac1 to the Golgi, where it dephosphorylates PtdIns4*P* to PtdIns. **(B)** Confocal images confirming PJ-Sac1 translocation from the cytoplasm to the giantin-FRB–enriched Golgi after 10 min with 1 µM rapamycin. Right: GFP-tagged OSH1, a PtdIns4*P* indicator, reports a reduction of Golgi PtdIns4*P*. Scale bar, 10 µm.

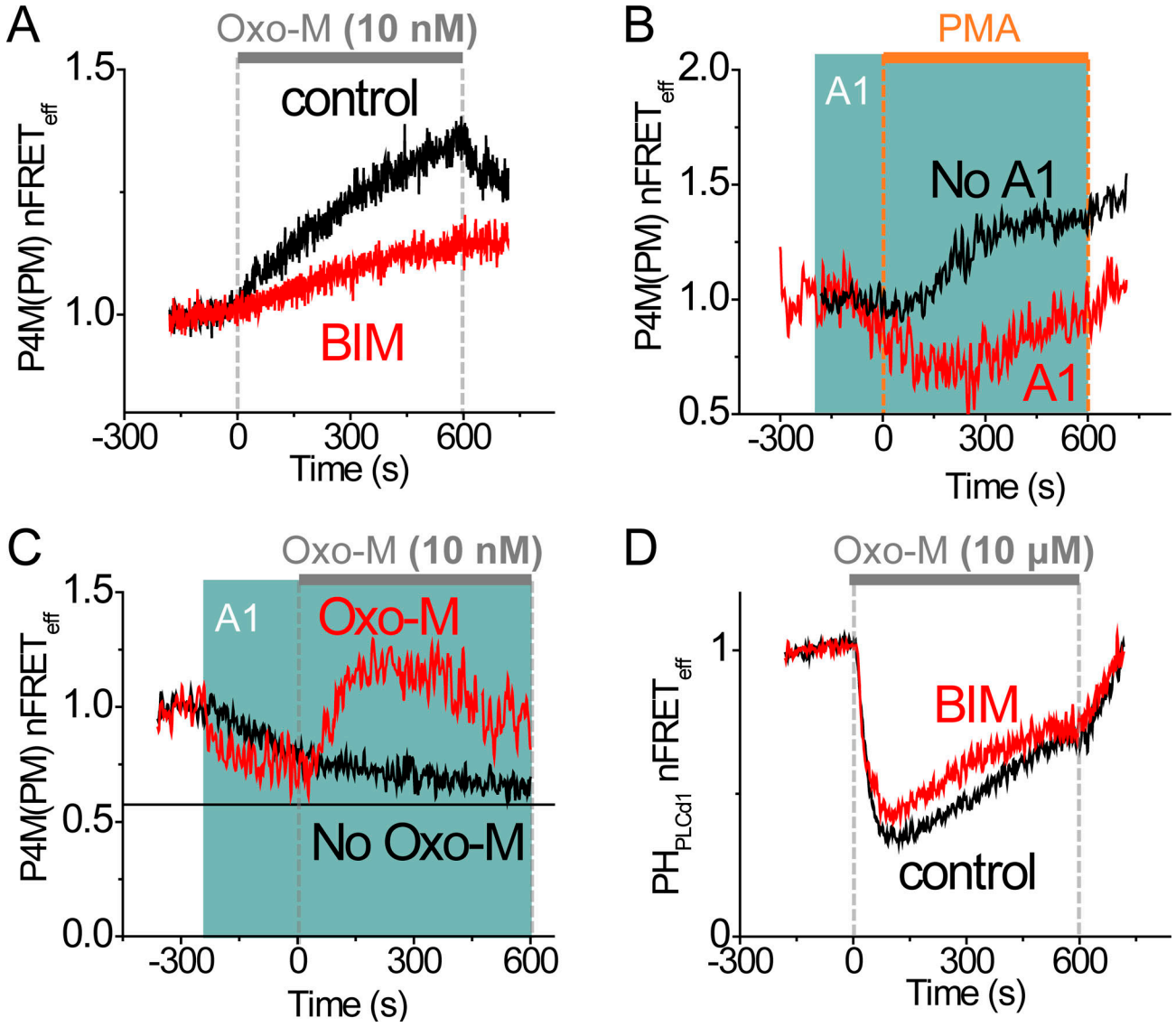

Figure S8. **Dissecting dynamics of phosphoinositide pools with drugs acting on PKC or PI4KIIIα. (A)** Time course of heterologous nFRET$_{eff}$ between P4M-CFP and Lyn-YFP in control cells and cells preincubated in 2 µM BIM during stimulation with a very low concentration of Oxo-M (10 nM, gray bar). **(B)** Increase of PM PtdIns4*P* concentration by application of 5 µM PMA (orange bar) with or without pretreatment with A1 (green shading), a specific PI4KIIIα inhibitor. **(C)** Pretreatment with 30 nM A1 initiated a loss of PM PtdIns4*P*, but 10 nM Oxo-M still stimulated PM PtdIns4*P* production. **(D)** Control cells and cells preincubated in 2 µM BIM expressing PtdIns(4,5)P_2 FRET probes showed regeneration during receptor activation by 10 µM Oxo-M.

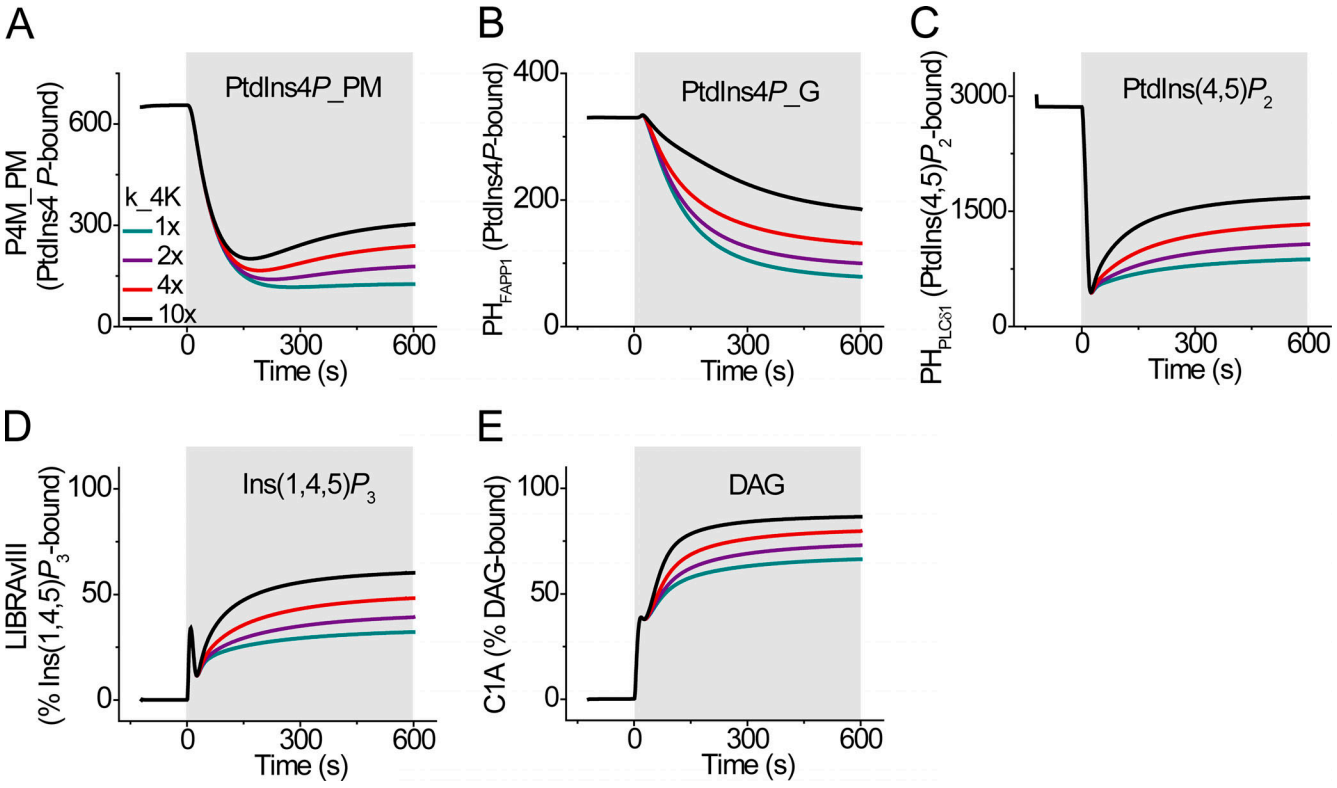

Figure S9. **Simulated dynamics of phosphoinositide probes during receptor activation (shaded area) using the expanded mathematical model. (A–E)** The rate constants for PI4K activity are varied as in Fig. 7 A. Corresponding simulated time courses of concentration of PM PtdIns4*P*-bound P4M (A), Golgi PtdIns4*P*-bound PH_{FAPP1} (B), PM PtdIns(4,5)P_2-bound $PH_{PLC\delta1}$ (C), Ins(1,4,5)P_3-bound LIBRAvIII (D), and DAG-bound C1A (E). _G indicates chemical species in the Golgi compartment.

Provided online are four tables. Table S1 lists the initial conditions and parameters for the model shown in Fig. 4. Table S2 describes the differential equation for the model shown in Fig. 4 Table S3 lists the initial conditions and parameters for the model shown in Fig. 7 and Fig. S9. Table S4 describes the differential equations for the model shown in Fig. 7 and Fig. S9.